Chapter 3: Curiosity driven study of Self Aggregation

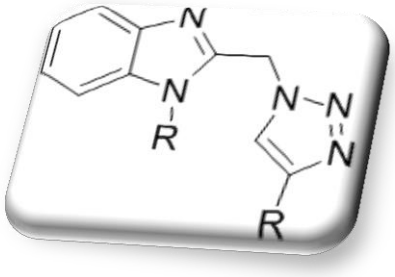

Abstract:

An interesting observation was made in chapter 2.2. While recording NMR, the solution inside the NMR tube got solidified. Why did the compound, having benzimidazole linked triazole parmacophore, remained in NMR tube after 12 hours and showed gel like or semisolid behavior? Some questions came up then. Is this a simple aggregation? Is it due to impurity? Is it common in literature? Can we see this behavior by changing other physical parameters, such as change in solvent system, temperature? Is it possible to trace 'molecular' origin for such behavior? Many such questions will be answered in this chapter with the help of microscopic, thermal, single crystal and NMR studies. Designing of the molecules was based on three facts: 1. Check the effect of phenyl/aniline linkers 2. Check the effect of floro/non-florogroups 3. Check the effect of ethyl/non-ethyl group. Firstly, the real time images were captured with polarizing optical microscopy for self aggregation. A microscopic study concluded that the growth of fibers is sperulitical initially and then fibrillar with both tip branching and side branching. The fibers obtained from DMSO are much thicker as compared to water addition fibers. Thermal analyses TG-DTA and DSC were performed for understanding the stability and phase transitions, if any, for the molecules under consideration. We observed that the three representative molecules showed phase transitions at above 100°C. Successfully single crystal was obtained for two ethyl derivatives while for other derivatives we didn't get any. Single crystal XRD was performed for getting more insight to the various interactions in solid phase. COSY and HSQC NMR measurements were used for the complete assignment of proton signals for all the newly synthesized eight benzimidazole linked triazole molecules in solution. Concentration dependent and titration with water of proton chemical shifts of the molecules under consideration were measured. Concentration dependent and water addition NMR experiments revealed the specific shifting of protons, such as methylene bridges, *ortho*-protons of the phenyl ring. Thus, these protons were probable candidates for aggregation or self-aggregation behavior. Close-contact in Single crystal XRD studies and thermal data supports our NMR conclusions. The fibers were stable at room temperature for more than a week's time and their formation is thermoreversible.

3.1 Curious observation:

This chapter deals with the un-usual behavior of benzimidazole and triazole adducts observed earlier in chapter 2.2, it was found that DMSO solution was getting solidified. The initial hypothesis was that it might be due to the gel formation, but after exploring the system it was observed that, it is not a gel but a self aggregation of the molecules. *Figure 3.1* shows the image of self aggregated fibers isolated from DMSO for 1-ethyl-2-((4-(4-fluorophenyl)-1*H*-1,2,3-triazol-1-yl)methyl)-1*H*-benzo[*d*]imidazole.

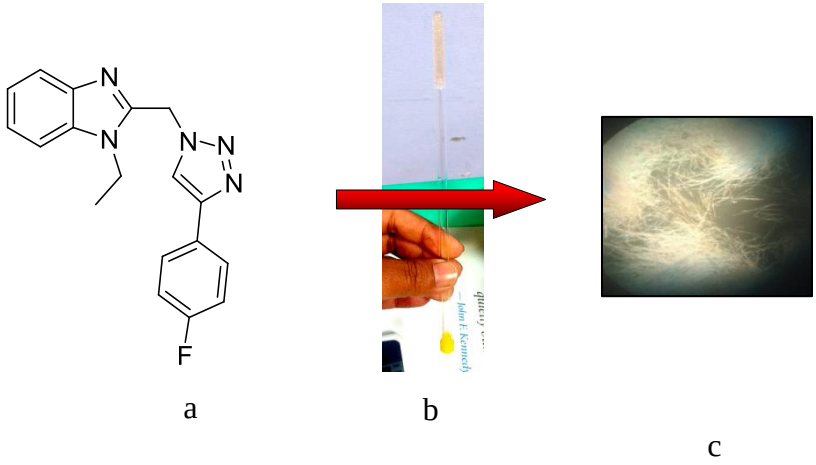

Figure 3.1: Serendipitous white solidification observed in NMR tube (a), for benzimidazole-triazole adducts (b) and under microscope (c)

Further investigations helped conclude that aggregation is possible in two ways: (i) addition of water in clear solution of DMSO (water addition) and (ii) keeping sample for various times in a neat DMSO solution (concentration dependent). It was observed that self aggregation was thermo reversible. For example when fibers, generated from water addition, were heated (in solution phase) the transition from aggregated solid state to clear liquid state was observed at 70°C for 1-ethyl-2-((4-(4-fluorophenyl)-1*H*-1,2,3-triazol-1-yl)methyl)-1*H*-benzo[*d*]imidazole:

Self Aggregation $\underset{\longleftarrow}{\overset{\text{Heating}}{\longrightarrow}}$ Dissolved State

Curiosity then forced for further investigation. The first step was to establish the structure activity relationship for our observation. Thus, eight different derivatives were designed, out of which five derivatives were from chapter 2.2 and the other three were synthesized

(*Figure 3.2 and 3.3*). Synthesis proceeded the same way we did for rest five compounds (Scheme 3.1).Designing was based on three facts: (i) check the effect of phenyl/aniline linkers (ii) check the effect of floro/non-florogroups (iii) check the effect of ethyl/non-ethyl groups.

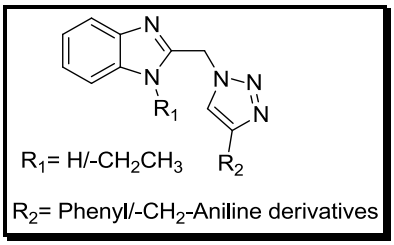

Figure 3.2: Schematic representation of derivatives of benzimidazole-triazole adducts

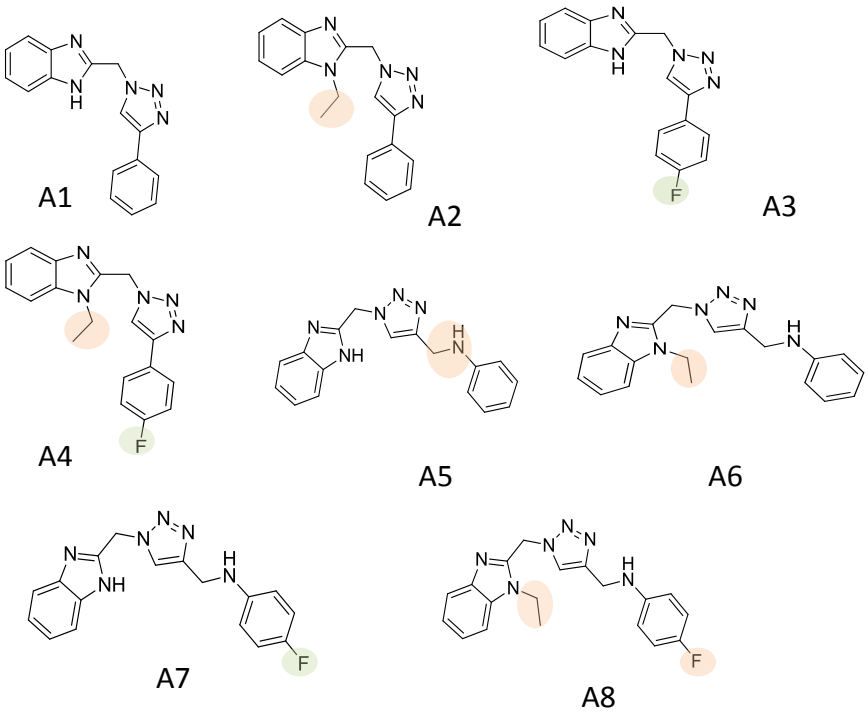

Figure 3.3: Benzimidazole-triazole adducts considered for investigation

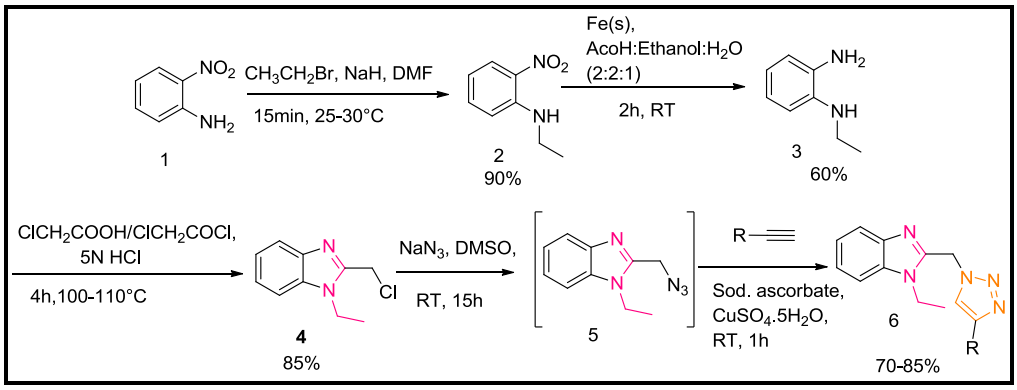

Scheme 3.1: Synthesis of *N*-((1-((1-ethyl-1*H*-benzo[*d*]imidazol-2-yl)methyl)-1*H*-1,2,3-triazol-4-yl)methyl)aniline and its derivatives

Three new benzimidazole-triazole adducts were synthesized by click chemistry of an azide-containing substituted benzimidazole ring with phenylene or aniline carrying a triple bond functionality to give benzimidazole-triazole adducts (*Scheme 3.1*). The synthesis was carried out in a similar fashion as was discussed in chapter 2.2. In totality eight molecules were considered for the investigation, out of which five molecules were taken from the chapter 2.2 and the other three were new molecules synthesized using the same strategy as shown in *Scheme 3.1*.

The successful synthesis of the molecules **A1** to **A8** benzimidazole-triazole adducts was confirmed by ^{1}H and ^{13}C nuclear magnetic resonance (NMR) spectroscopic analysis. Single-crystal X-ray diffraction further confirmed the right structure and gave information concerning the supramolecular arrangement of the triazole molecules into tridimensional architectures.

Pure molecules **A1** to **A8** were charged in a glass vial. DMSO was added to obtain a clear solution. Water was then added to get the self aggregation. *Table 3.1* summarizes the exact quantity used for the experiments. For **A8** the self aggregation was not instantaneous after water addition but took an overnight's time instead.

Table 3.1: Experimental values for self aggregation

Structure	Amount (mg)	DMSO (ml)	Water (ml)	Total solvent (mg)
A1	10	0.1	0.032	142.4
A2	10	0.1	0.032	142.4
A3	10	0.1	0.032	142.4
A4	7	0.1	0.032	142.4
A5	10	0.1	0.162	272.0
A6	10	0.1	0.097	207.2
A7	10	0.1	0.064	174.8
A8	10	0.1	0.064	174.8

Figure 3.4 presents the images that we captured for our experiment. The glass vials as shown in *Figure 3.4* in the last Figure were made to be inverted as a part of gel test and we observed that the solution was immobilized. With this the systematic investigation was started.

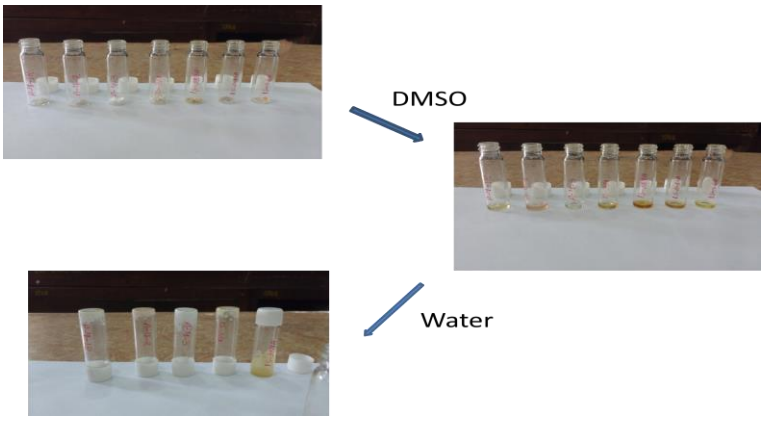

Figure 3.4: Experiment showing aggregation

Literature shows many reports on low molecular mass organic gelators (LMOGs) and supramolecular gelators for aqueous DMSO [1]. Yu et al. reported supramolecular gels using surfactants based on imidazolium salts in aqueous DMSO [2]. Yang et al. developed Fmoc-derived naphthalene modified peptides gelators from aqueous DMSO solution [3]. Wang et al developed sugar based low molecular weight gelators for aq. DMSO. They observed that N-linked carbamates are good gelators for aq. DMSO solutions [4]. Glycosyl linked triazoles analogs containing long alkyl hydroxyl groups and phenyl groups typically are effective in forming supramolecular gels was discussed by Mangunuru et al [5]. 1D structure which is formed initially is further converted to 3D structures forming self assembled fibrillar networks (SAIFs) [6]. LMOG molecules in fibers are not attached covalently, but with H-bonding, π-π stacking, dipolar interactions and London dispersion forces [7]. Considering the binary solvent mixture of DMSO and water in this case, many theories of their interactions amongst themselves solvent-solvent is observed in the literature [8]. At high concentration of DMSO the formation of stable 3DMSO:1water complexes are suggested, in which the water molecule is shielded from the surroundings. The formation of 1DMSO:2Water trimmer is also reported where water oxygen atoms interact with sulfoxide methyl groups [9].

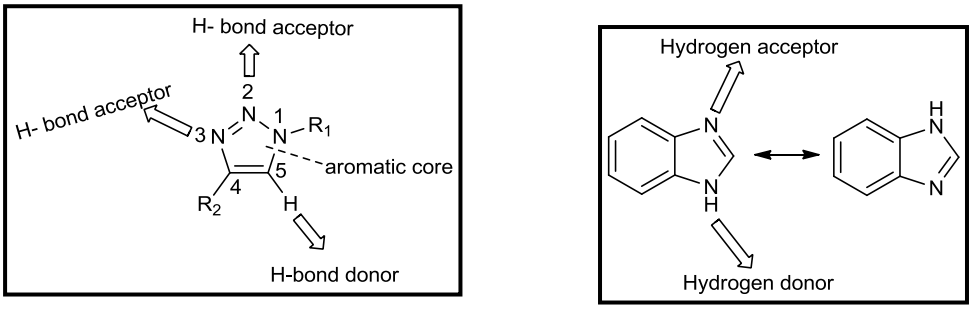

Figure 3.5: Donor acceptor sites for triazole and benzimidazole

Triazole and benzimidazole having e- rich and poor sites in the molecular structure are good candidates for intermolecular self assembly (*Figure 3.5*). Solute and solvent interaction in our case can be because of hydrogen bonding or other weak forces. All these solute-solvent and solvent-solvent interactions may be playing a crucial role in self assembly.

Reason for gelation or self aggregation property of benzimidazole has been extensively reported in literature [10-12]. The reason behind this is due to their unique ability to form π-π stacking and vanderwaals interaction [13-15]. The discovering of small organic molecules capable of forming gel is an expanding research area due to their possible applications in tissue engineering, drug delivery vehicles and pollutant removal machineries [16-18]. It has been noted that gel formation is closely related to molecular self assembly. To understand the structure of self aggregation it can be divided into primary, secondary and tertiary structures, like protein structure (*Figure 3.6*) [16]. Primary structure is derived from the interaction of molecules amongst themselves using hydrogen bonding or other weak forces, leading to one dimensional or two dimensional aggregation assemblies. Secondary structures is defined as the morphology of the aggregates that is, micelles, vesicles, fibers, ribbons or sheets and is directly influenced by the molecular structure. Lastly tertiary structure deals with the interaction of the aggregates formed; three dimensional structure [16].

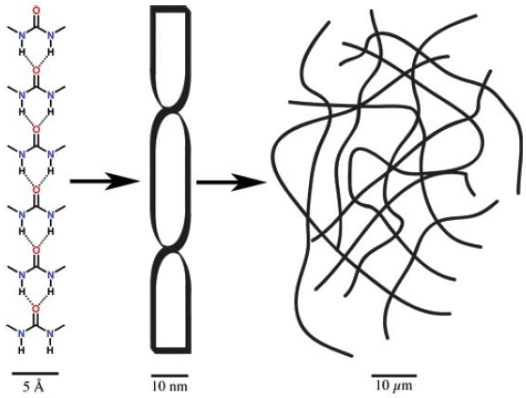

Figure3.6: Primary, secondary and tertiary structure of self aggregates (Figure adapted from reference 1)

The molecular gel formed is believed to be formed solely with the help of non-covalent forces. Thermo reversibility is the characteristic feature to distinguish the molecular gels from the covalent force mediated chemical gels [19]. The fiber network structure can be described by considering junctions and edges (*Figure 3.7*). The junctions can be further classified into two sub structures; i.e transient junction and permanent junction [20-21]. Further permanent junctions includeside branching and tip branching [20,22].

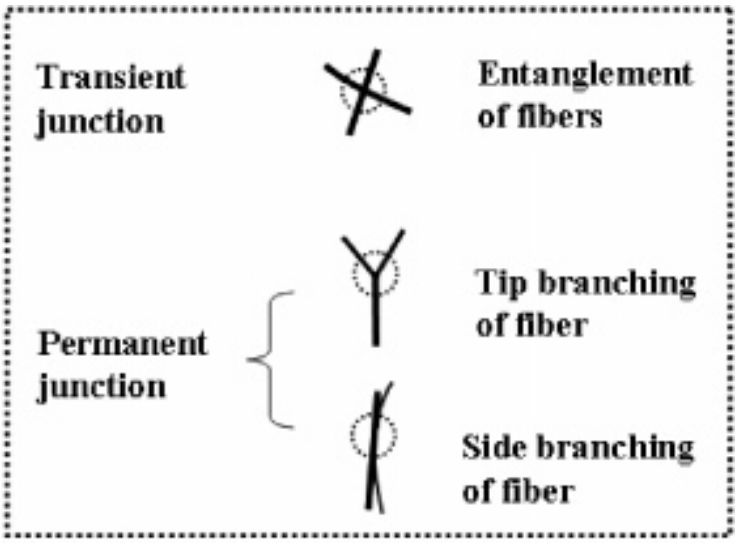

Figure3.7: Schematic of fiber network and nature of junctions (Figure is adapted from ref 4)

Nucleation of individual fibers can occur under low supersaturation-where fibers grow in one dimension with less branching and under high supersaturation condition facilitating growth of a densely branched morphology, also known as spherulitic growth (*Figure3.8*) [19]. Hence these observations give idea about the self assembly which further helps in understanding the microstructure.

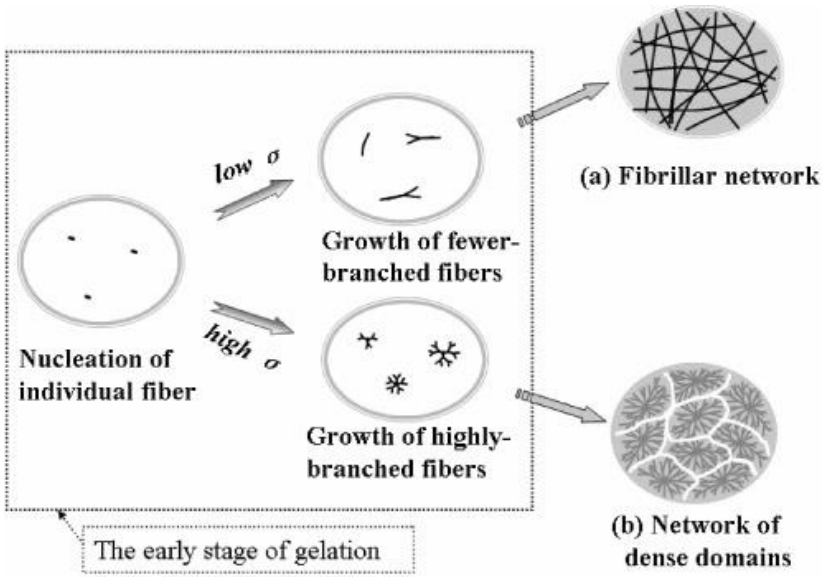

Figure3.8: Schematic representation of growth of gel (a) fibrous growth (b) spherulitic growth (adapted from refer 4)

To exploit the observations made by us in the earlier part of this section, there was a curiosity to know more about the phenomenon of self assembly. For this five objectives were formulated to investigate these aggregation phenomena:

Objective 1: Images for self aggregation using polarizing optical microscopy (POM)

Objective 2: Thermal analysis (TG-DTA and DSC)

Objective 3: Single crystal XRD analysis

Objective 4: Labeling of the protons in the structure using COSY and HSQC.

Objective5: Systematic NMR studies (Concentration as well as water addition experiment)

3.2 Objective 1: Microscopic Images using POM

To get insights into the self aggregated fibers, it was mandatory to capture images at various stages after water addition using polarizing optical microscopy (POM). Systematic study for this was performed.

1. Images of 2-amino benzimidazole

   To visualize the molecule in a better way, we planned the experiment for commercially available 2-amino benzimidazole and benzimidazole. On a glass slide we dissolved 2-amino benzimidazole in DMSO and then added drops of water until hazy. The images below we see appear to be plate like. Images 1 and 2 were captured at 4X magnification. Image 3 is at 10X magnification (*Figure 3.9*).

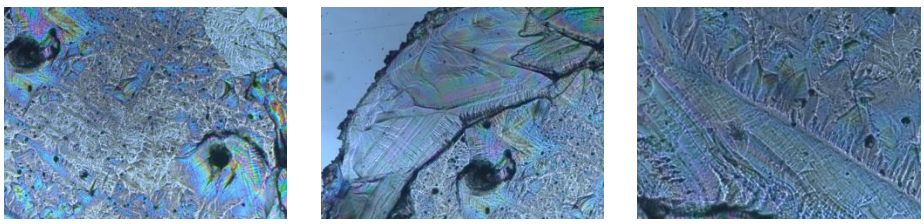

Image 1 at 4X Image 2 at 4X Image 3 at 10X

Figure 3.9: POM images for 2-amino benzimidazole

2. Images of benzimidazole

   In case of benzimidazole same experiment was performed as in the previous section. As can be seen images, benzimidazole after water addition can be seen in various forms, such as cube and plate like. Image 1 is at 4X magnification and image 2 is at 10X magnification (*Figure 3.10*).

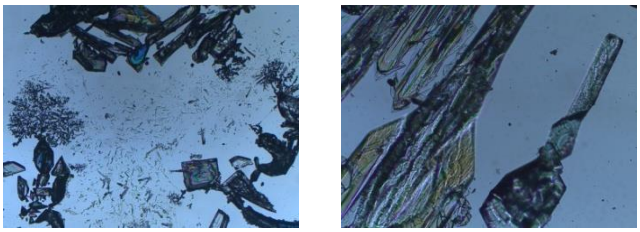

Image 1 at 4X Image 2 at 10X

Figure 3.10: POM images for benzimidazole

3. Images of **A2**

   On a glass slide molecule **A2** was taken and then a drop of DMSO was added to get a clear solution (Image 1). A small drop of water was added (Image 2). Image 3 shows immediate starting of self aggregation process. Within no time we observed spherulitic thick fiber like structures with tip branching and side branching (*Figure 3.11*).

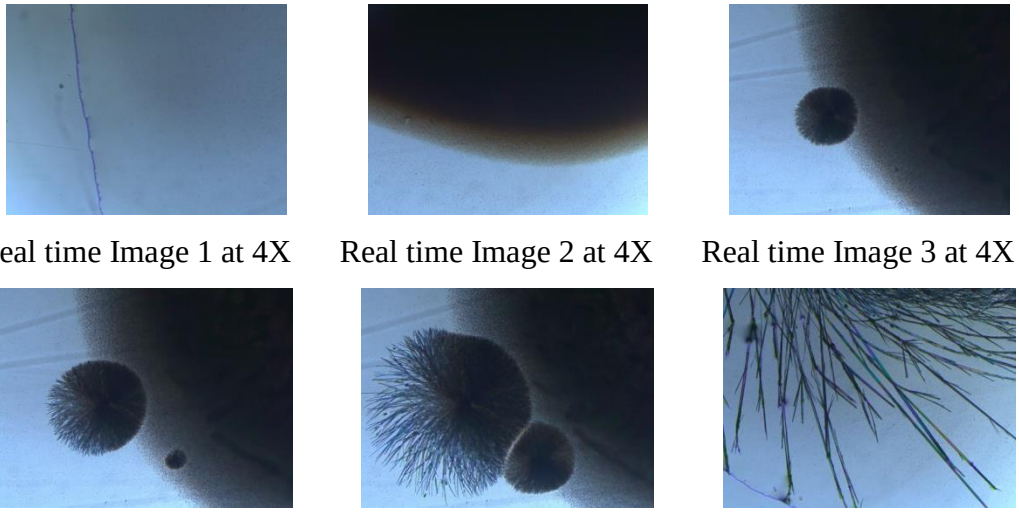

Real time Image 1 at 4X Real time Image 2 at 4X Real time Image 3 at 4X

Real time Image 4 at 4X Real time Image 5 at 4X Real time Image 6 at 4X after 5 mins

Figure 3.11: POM images for A2

4. Images of **A3**

For this molecule we recorded images for three different cases.

Case 1: The solid was taken on a glass slide and images at various magnifications were captured. Small thread like structures was observed (Images 1 to 3, Figure 3.11).

Case 2: Pre-prepared isolated fibers on the glass slide were placed and then images were captured. Thick long fibers can be seen with tip and side branching (Images 4 to 7, *Figure 3.11*).

Case 3: Real time images for the self aggregation after water addition were captured. Image 8 here shows clear solution of molecule under consideration. Image 9 shows the immediate self aggregation after water addition. Images 10and 11 gives the magnified images of the fiber (Images 8 to 11, *Figure 3.12*). Here fibrillar growth dominated.

Image 1 at 4X for solid

Image 2 at 10Xfor solid

Image 3 at 20X for solid

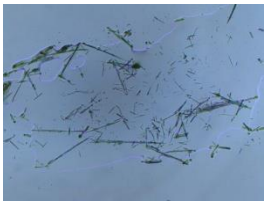

Image 4at 4X for isolated fibers

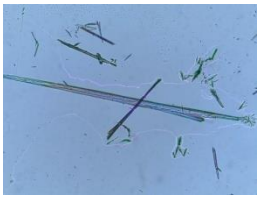

Image 5 at10X for isolated fibers

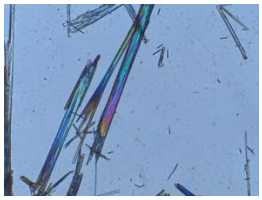

Image 6 at 20X for isolated fibers

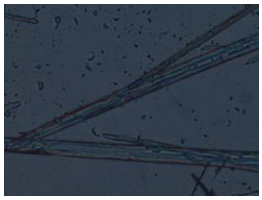

Image 7 at 50X for isolated fibers

Real time image 8 at 4X

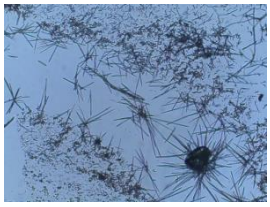

Real time image 9 at 4Xafter 5mins

Image 10 at 10X

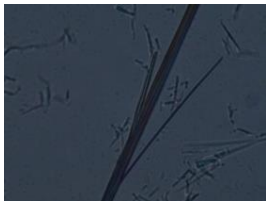

Image 11 at 50X

Figure 3.12: POM images for A3

5. Image of **A4**

   For this molecule images were captured in the following cases:

   Case 1: Self aggregation with only DMSO was allowed to occur on the slide and then images of dried fibers (overnight) were captured at various magnifications (Images 1 to 4, *Figure 3.12*).

   Case 2: Images of solid compound. Here, small threads of the compound can be seen (Images 5 to 7, *Figure 3.12*).

   Case 3: Water addition experiment. Image 8 gives a clear picture of dissolved molecule in DMSO. Image 9 is captured just after water addition. Image 10 shows immediate self aggregation after water addition. Here small spherulitical growth leading to small fibers is observed (Images 8 to 10, *Figure 3.13*).

Image 1 at 4X

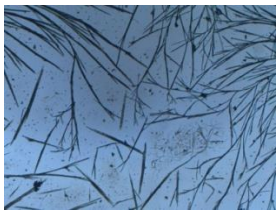

Image 2 at 4X

Image 3 at 10X

Image 4 at 20X

Image 5 at 4X for solid

Image 6 at 10X forsolid

Image 7 at 20X forsolid

Real time image 8 at 4X

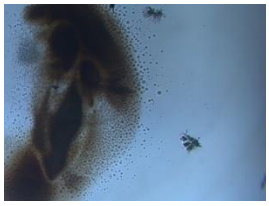

Real time image 9 at 4X

Real time image 10 at 4X after 3mis

Figure 3.13: POM images for A4

6. Image of **A6**

For this molecule Image 1 to 4 shows real time images (*Figure 3.14*). Image 2 is captured just after water addition. Here immediate self aggregation spherulitical formation can be seen. Consecutive images are for the fibers formed at different magnification (*Figure 3.14*).The fibers here shows both tip branching and side branching.

Real time image 1 at 4X

Real time image 2 at 4X

Real time image 3 at 4X

Real time image 4 at 4X after 5 mins

Image 5 at 10X

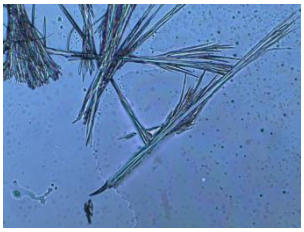

Image 6 at 20X

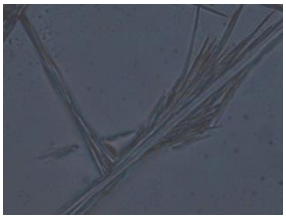

Image 7 at 50X

Figure 3.14: POM images for A6

Overall conclusion from imaging: It was observed that for floro phenyl derivatives (**A3** and **A4**), the fibers were of comparatively smaller size even after 30mins. For **A2** and **A6** significantly bigger fibers were observed just after 5mins of water addition. Growth of fibers in all cases was observed as initially sperulitical (just after addition of water) and then fibrillar (after 2 or more mins), but for **A4** we observed only sperulitical growth. Also for **A3** the growth is fibrillar.

3.3 Objective 2: Thermal analysis

Second objective was the thermal analysis for the molecules. TG-DTA for solid **A3** phase transition was observed at around 200°C followed by two mass losses, first one at below 100°C and second one in the range of 220-380°C (*Figure 3.15*). For **A4** the phase transitions in TG-DTA was observed at around 135°C and 150°C, which is also observed in DSC spectra (*Figure 3.16* and *3.17*). In addition, DSC gives an endotherm at 123°C while cooling, suggesting that this phase transition is reversible. TG-DTA of **A4** reveals two mass losses one at around 150°C and the second between 210-360°C (*Figure 3.17*). For **A6** the analysis was done in its crude solid form (*Figure 3.18*) and after self aggregation on water addition (*Figure 3.19*); the fiber like structure was isolated and without drying was used for further analysis. As from TG-DTA for solid crude **A6** phase transition at around 125°C was observed, which is also observed in DSC graphs. The TG-DTA for solid **A6** shows the thermal stability of the molecule upto 220°C and after that decomposition is observed till 360°C, complete decomposition was observed. From TG-DTA spectra of self aggregated assembly (*Figure 3.20*), it shows a big mass loss before 100°C and we can observe phase transition at 125°C with second mass loss from 250-350°C. From the two TG-DTA graphs it can be concluded that the molecules in self aggregated form has not lost its identity and may be the weak forces in its primary structure is responsible for the fiber formation. DSC graphs for **A6** solid (*Figure 3.20*) and self aggregated **A6** (*Figure 3.21*), shows that phase transitions at same temperature which gets broadened in the fiber form, typical of self aggregation phenomenon. Conclusion from thermal analysis is that we observed phase transitions for all the three representative compounds (**A3**, **A4** and **A6**), which is also observed in DSC.

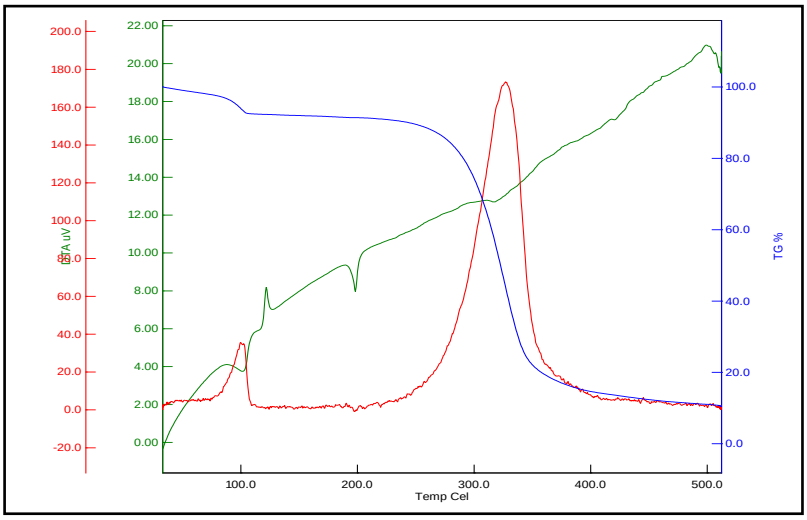

Figure 3.15: TG-DTA of solid A3

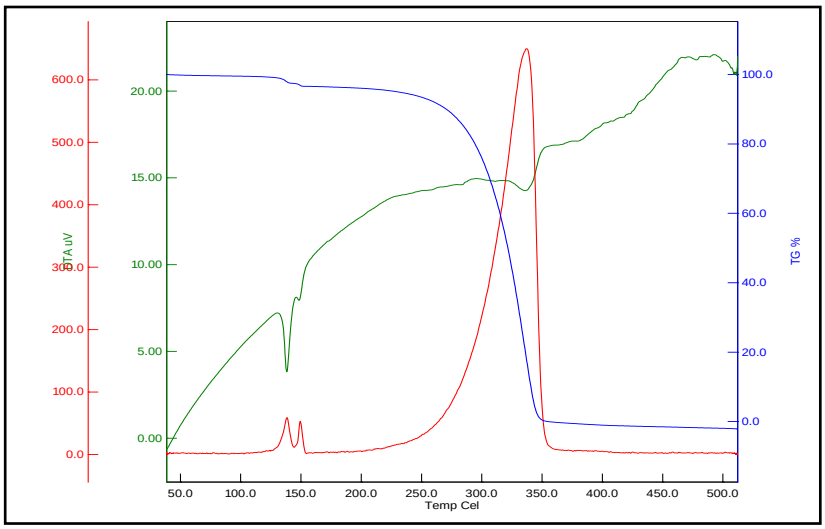

Figure 3.16: TG-DTA of solid A4

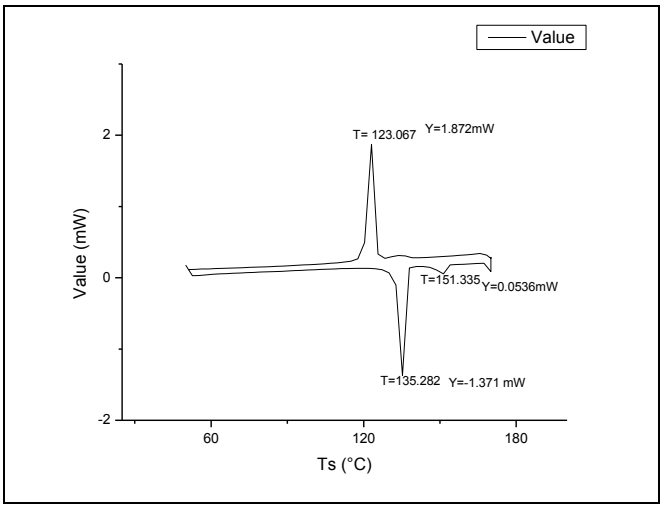

Figure3.17: DSC of solid A4

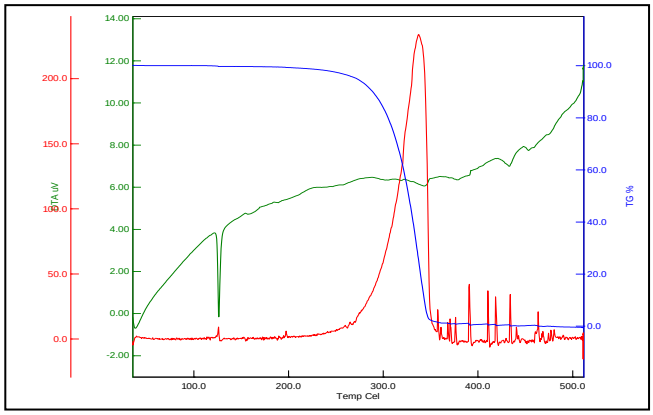

Figure 3.18: TG-DTA of solid A6

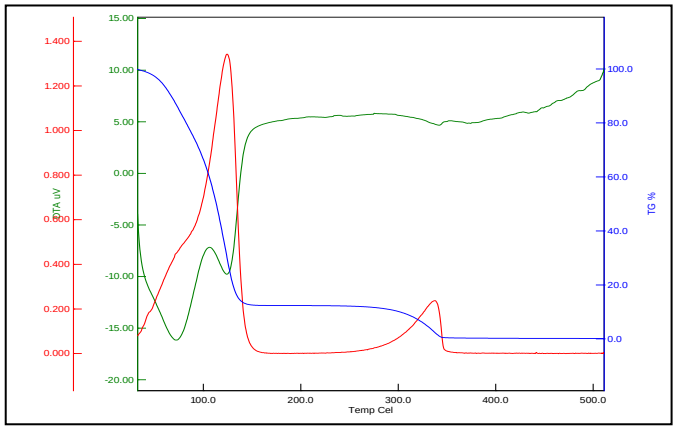

Figure 3.19: TG-DTA of A6 after water addition: Self assembly

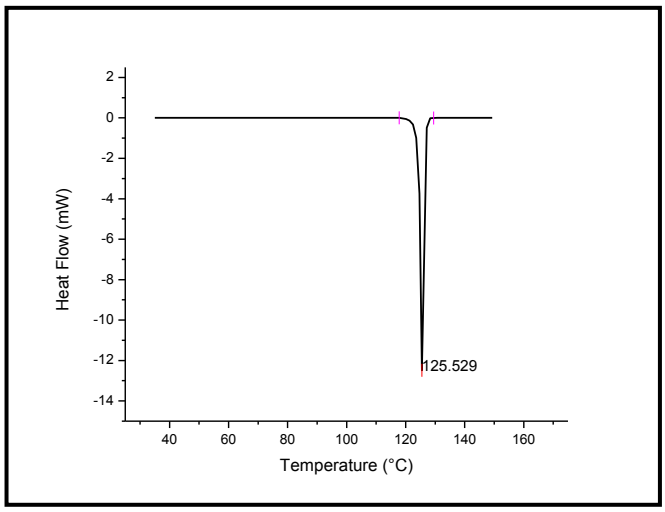

Figure 3.20: DSC of A6

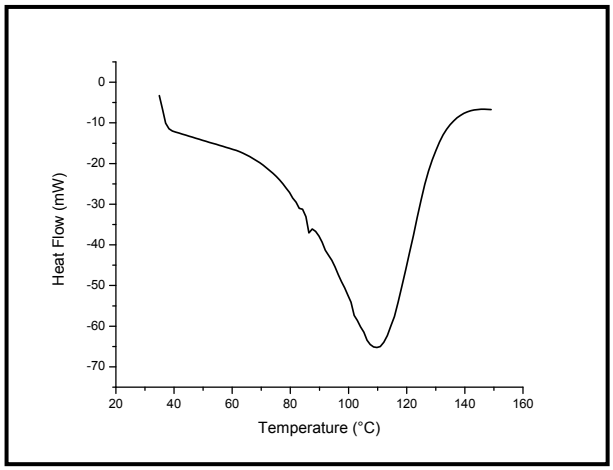

Figure 3.21: DSC of A6 after addition of water: self assembly

3.4 Objective 3: Single crystal XRD

Single crystals were developed for **A2** (ethyl phenyl) and **A6** (ethyl aniline) using slow evaporation technique from ethylacetate and petroleum ether as solvent. As reported in table 3.2, molecule **A2** gets crystallized in triclinic crystal system with *P-1* space group and molecule **A6** gets crystallized in orthorhombic crystal system with $Pna2_1$ space group.

Table 3.2: Crystallographic data and structure refinements for A4 and A6

	A2	A6
CCDC	1828854	1544619
Empirical formula	C18 H16 N5	C19 H20 N6
Formula weight(g M^{-1})	302.36	332.41
Crystal system	triclinic	Orthorhombic
Space group	*P -1*	*P n a* 2_1
***a*(Å)**	4.7443(6)	20.043(3)
***b*(Å)**	12.7791(16)	16.153(2)
***c*(Å)**	13.2626(16)	5.4654(7)
***α*(°)**	103.724(11)	90.0
***β* (°)**	92.612(10)	90.0
***γ* (°)**	94.659(10)	90.0
***V* (Å^3)**	776.80(17)	1769.4(4)
Z	2	4
***T* (K)**	273(2)	273 (2)
ρ_{calc}(g cm^{-3})	1.2926	1.248
***λ* (Å) (Mo-K*α*)**	0.71073	0.71073
***μ* (cm^{-1})**	0.770	0.770
Data/restraints/parameters	3500/0/208	4059 / 1 / 226
***F* (000)**	318	565
Goodness-of-fit	1.0775	1.020

3.4.1: Single Crystal study of A2

The X-ray study of the floro phenyl ethyl derivative **A2** reveals that the molecule has 90° twisted X shap, sitting on the lower arms of X by making an angle of 84.74° (*Figure 3.22 to 3.24*). X-ray structure reveals the interaction between triazole ring of one molecule and CH_2 linker having average distance of 3.34Å which propagates along *a*-axis. The second interaction exists between triazole ring and methyl of ethyl group with a distance of 3.61Å which propagates along *a*-axis. The next interaction exists between the *ortho* and *meta* hydrogens of the phenyl ring with distance of 3.65Å propagating towards *c*-axis.

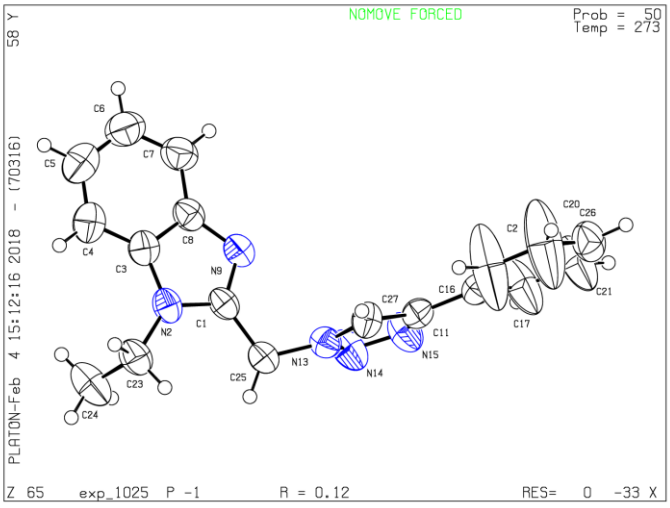

Figure3.22: Molecular view of compound A2 having thermal ellipsoid are shown with 50% probability

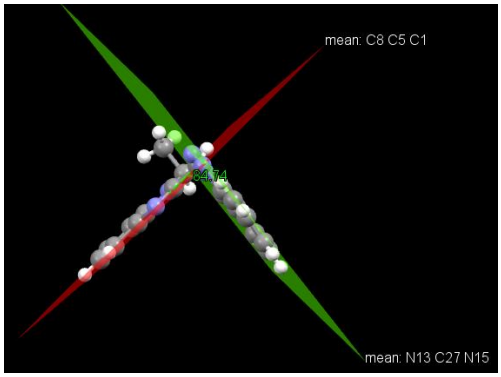

Figure3.23: Molecular view of A2 showing the inter planar angle of 84.7°

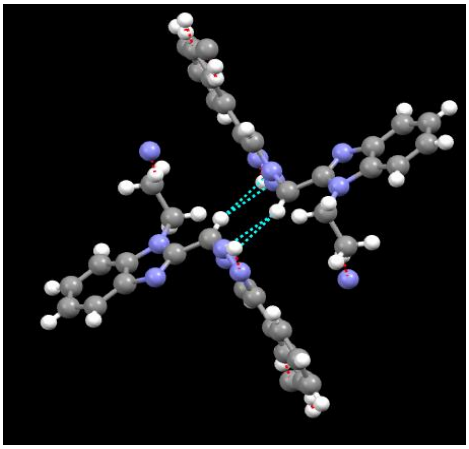

Figure3.24: Molecular view of A2 showing the vanderwaal interaction between two neighbor molecules

3.4.2: Single crystal study of A6

From the X-ray diffraction study of **A6**, the fact that each molecule adapted a tweezer like shape emerged (*Figure 3.25 and 3.26*), with a near parallel alignment of the two fragments borne by the triazole ring (87.10° and 86.01°). Despite their proximity, the benzimidazole and phenyl ring atoms do not interact (5.39Å); indeed they are involved in short contacts with the neighboring molecules. The ethyl groups are oriented towards the inner side of the tweezer which minimizes the repulsion for the intermolecular arrangement and gives it perfect orientation for self assembly. One molecule shows seven short contacts. Both the CH_2 linkers participate in the non-covalent interactions with the distance of 3.33Å and 3.42Å for CH_2 benzimidazole linker and 3.61Å and 3.69Å for CH_2 aniline linkers. The nitrogen of the imidazole ring is attached with *o*-carbon and CH_2 aniline linker of the other molecule at a distance of 3.69Å and 3.91Å respectively. A continuous propagation of contact between C_5-N_2 (3.33Å) of triazole ring is observed along *c*-axis.

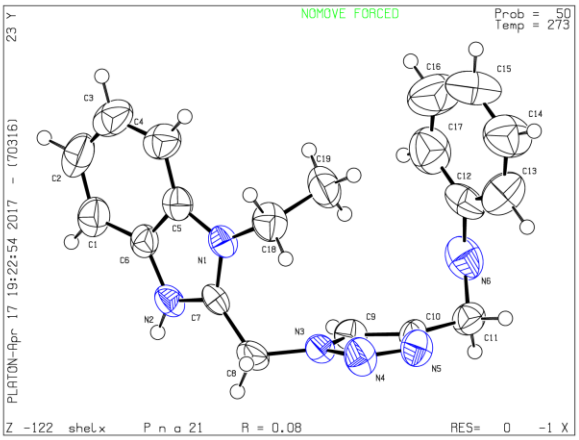

Figure3.25: Molecular view of compound A6 having thermal ellipsoid are shown with 50% probability

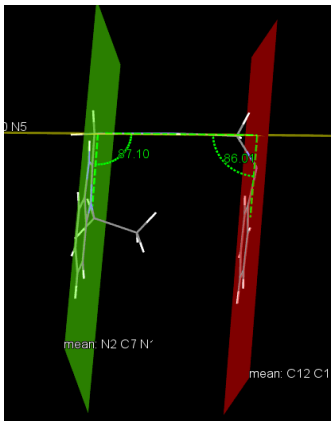

Figure3.26: Molecular view of A6 showing the parallel planes

3.5 Objective 4: Labeling of protons using 2D NMR techniques

Last two objectives for our study were to assign the labeling to the protons using 2D NMR and systematically study NMR measurements in solution phase. As a representative, compound **A6** is discussed. Assignments of the protons were obtained from both correlation spectroscopy (COSY) and heteronuclear single-quantum correlation spectroscopy (HSQC) experiments (*Figure 3.27, 3.28* and *3.29*). Signal assignments obtained for all the non-exchangeable protons are in good agreement with the structure.

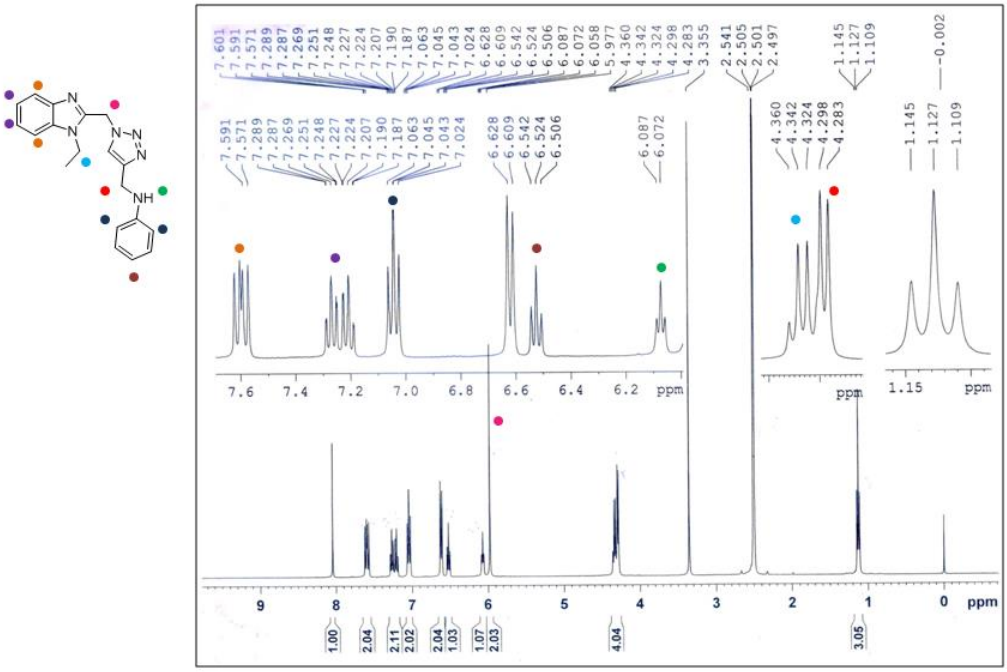

Figure 3.27: ^{1}H NMR of A6

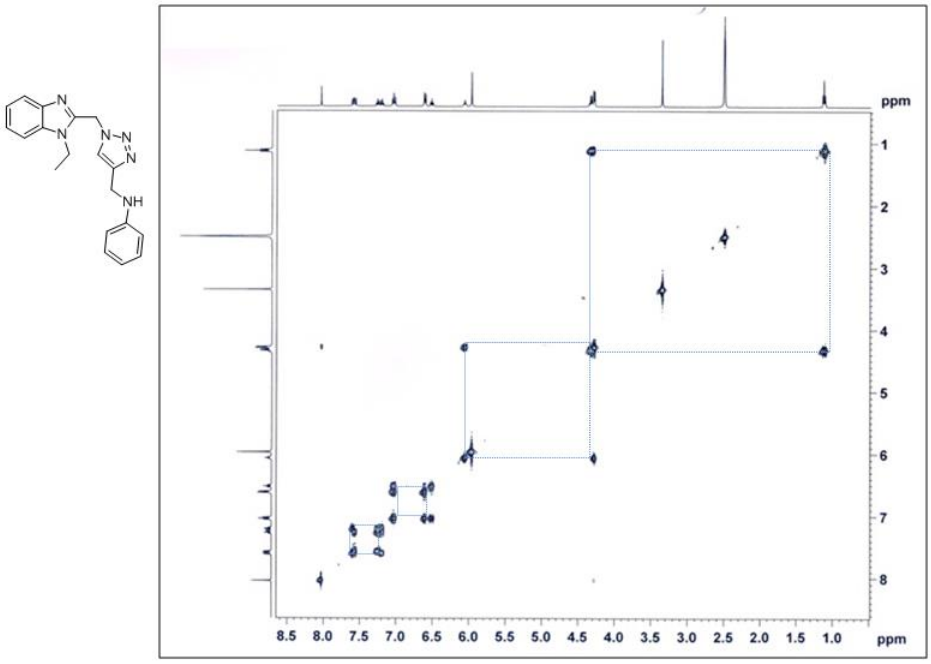

Figure 3.28: COSY NMR of A6

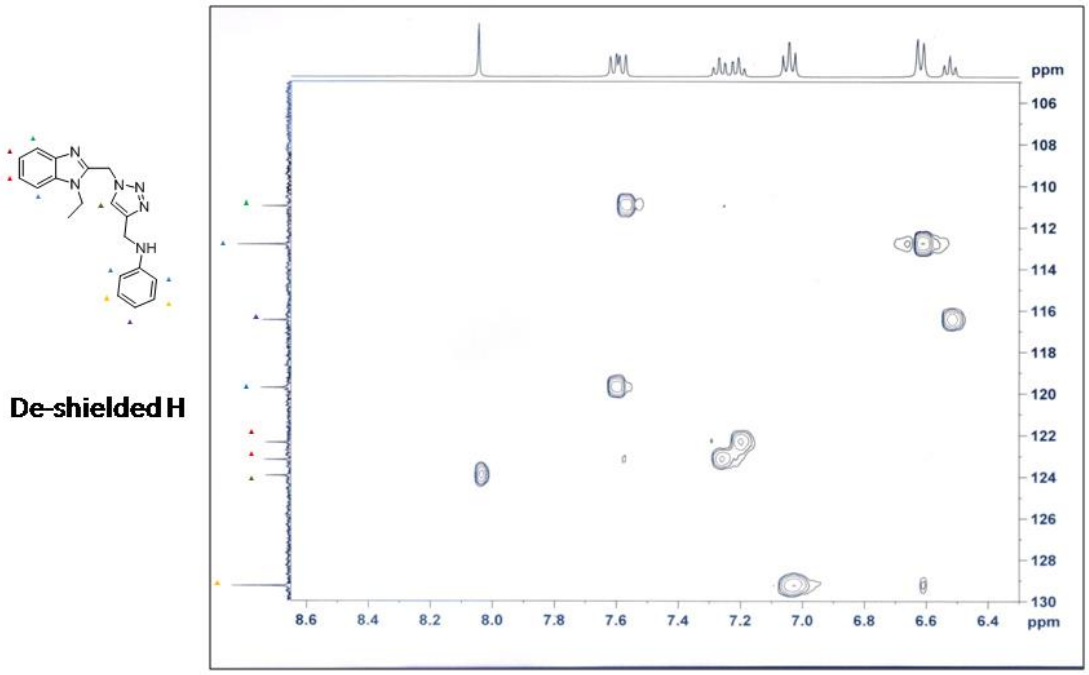

Figure 3.29: HSQC of A6

A. Molecule **A1**

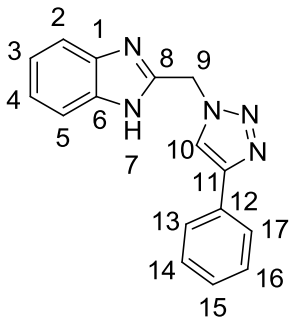	White solid. **Yield:** 78% **^{1}H NMR (400MHz,DMSO-d6) δ:**12.80 (s, H7), 8.72 (s, H10), 7.89-7.87 (m, H13,H17), 7.59 (s, H2,H5), 7.46-7.42 (m, H14,H16), 7.35-7.31 (m, H15), 7.19 (s, H3,H4), 5.92 (s, H9) ppm; **^{13}C NMR (100MHz, DMSO-d6) δ:** 153.5(C11), 151.8(C8), 135.7(C6), 134.2(C10), 133.3(C15), 130.4(C13,C17), 127.4(C3), 52.7(C9) ppm (*Figure 3.32, 3.33*)

B. Molecule **A2**

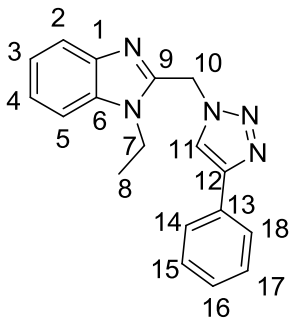	White solid. **Yield:**95% **^{1}H NMR (400MHz,DMSO-d6) *δ*:**8.70 (s, H11), 7.89-7.87 (d, H14,H18, *J*=7.2Hz), 7.63-7.59 (t, H2,H5, *J*=7.2Hz), 7.45-7.41(t, H15,H17, *J*=6.8Hz), 7.34-7.19 (m, H3,H4,H16), 6.08(s, H10), 4.40-4.38 (m, H7), 1.22-1.19(m, H8) ppm **^{13}C NMR (100MHz, DMSO-d6) *δ*:**148.35(C12), 147.14(C9), 142.52(C6), 135.26(C1), 130.99(C11), 129.36(C15,C17), 128.43(C13), 125.68(C14,C18), 123.21(C16), 122.67(C4), 122.38(C3), 119.75(C2), 110.99(C5), 46.57(C10), 38.82(C7), 15.26(C8) ppm (*Figure 3.34*, *3.35*,*3.36*, *3.55*)

C. Molecule **A3**

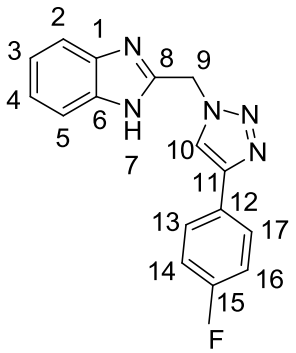	White solid. **Yield:**>98% **^{1}H NMR (400MHz,DMSO-d6) *δ*:**8.70 (s,H10), 7.94-7.90 (m, H13,H17), 7.55-7.53 (m, H2,H5), 7.31-7.27(t, H14,H16, *J*=9.2), 7.20-7.18 (m, H3,H4), 5.92 (s, H9) ppm; **^{13}C NMR (100MHz, DMSO-d6) *δ*:**148.7(C11), 146.2(C8), 127.7 and 127.6(C17, C13, 3JC-F=8Hz), 122.6(C3), 116.4 and 116.2(C14,C16, 2JC-F=2Hz), 48.0(C9) ppm;

	(*Figure 3.37, 3.38, 3.39, 3.40, 3.41*)

D. Molecule **A4**

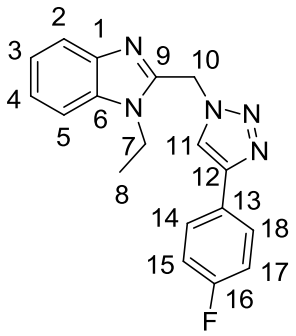	White solid. **Yield:**>98% **^{1}H NMR (400MHz,DMSO-d6) δ:** 8.70 (s, H11), 7.94-7.91 (m, H14,H18) 7.63-7.59 (t, H2,H5, *J*=7.6Hz), 7.30-7.25 (t, H4,H15,H17, *J*=8.4), 7.23-7.19 (t, H3, *J*=7.6), 6.08 (s, H10), 4.41-4.36 (q, H7, *J*=7.2Hz), 1.22-1.19 (t, H8, *J*=7.2) ppm; **^{13}C NMR (100MHz, DMSO-d6) δ:**163.5 and 161.0(C16, 1JC-F=242.9Hz), 148.3(C12), 146.2(C9), 142.4(C6), 135.2(C1), 127.7 and 127.6(C14,C18, 3JC-F=8Hz), 127.5(C11), 122.6(C3), 122.4(C4), 119.7(C2), 116.4 and 116.2(2JC-F=216Hz), 111.0(C5), 46.5(C10), 38.8(C7), 15.2(C8) ppm (*Figure 3.42, 3.43, 3.44, 3.45*)

E. Molecule **A5**

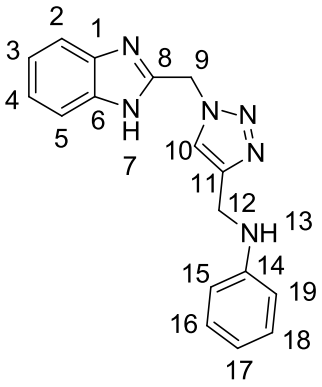	White solid. **Yield:** 90% **^{1}H NMR (400MHz,DMSO-d6) δ:**12.66(s, H7), 8.07(s, H10), 7.59-7.58(d, H2, *J*=7.2Hz), 7.50-7.48(d, H5, *J*=7.6Hz), 7.20-7.16(m, H3, H4), 7.07-7.03 (t, H16,H18, *J*=7.6Hz), 6.64-6.62 (d, H15,H19, *J*=8Hz), 6.55-6.51 (t, H17, *J*=7.2Hz), 6.08-6.05(t, H13, *J*=5.6Hz), 5.82(s, H9), 4.30-4.28(d, H12, *J*=6Hz) ppm; **^{13}C NMR (100MHz, DMSO-d6) δ:** 148.8(C14), 147.7(C8), 146.1(C6), 143.3(C1), 134.8(C11), 123.9(C10), 122.1(C3), 119.8(C16,C18), 119.4(C2), 114.2(C15,C19), 112.1(C5), 38.9(C9) ppm (*Figure 3.46, 3.47*)

F. Molecule **A6**

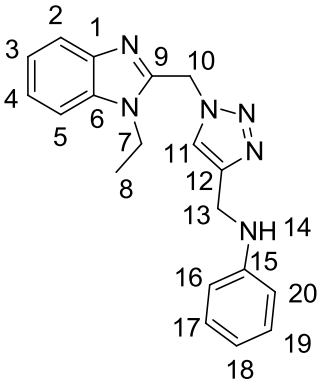	White solid. **Yield:**80% **^{1}H NMR (400MHz,DMSO-d6) δ:** 8.07 (s, H11), 7.60-7.57 (m, H2,H5), 7.28-7.18(m, H3,H4), 7.16-7.02 (t, H17,H19, *J*=7.2Hz), 6.62-6.60 (d, H16,H20, *J*=7.6Hz), 6.54-6.50(t, H18, *J*=7.2Hz), 6.08-6.05 (t, H14, *J*=6 Hz), 5.97 (s, H10), 4.36-4.28 (m, H7,H10), 1.14-1.10(t, H 8, *J*=7.2Hz)ppm; **^{13}C NMR (100MHz, DMSO-d6) δ:**148.7(C15), 148.4(C9), 146.6(C6), 142.4(C1), 135.1(C12), 129.2(C17,C19), 123.9(C11), 123.1(C4), 122.3(C3), 119.7(C2), 116.4(C18), 112.8(C16,C20), 110.9(C5), 46.1(C10), 38.7(C7),

	15.1(C8) ppm (*Figure 3.32, 3.33*)

G. Molecule **A7**

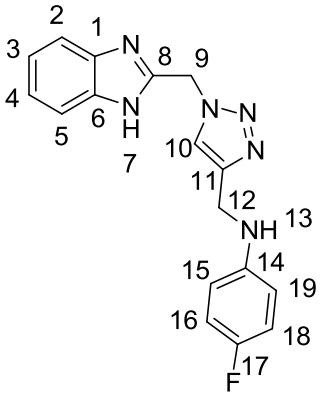	White solid. **Yield:**>98% **^{1}H NMR (400MHz,DMSO-d6) *δ*:**12.67(s, H7), 8.08(s, H10), 7.60-7.58(d, H2, *J*=7.6Hz), 7.50-7.48 (d, H5, *J*=7.6Hz), 7.22-7.14(m, H3,H4), 6.92-6.88(t, H16, H18, *J*=8.8Hz), 6.64-6.61(m, H15, H19), 6.03-6.00(t, H13, *J*=5.6Hz), 5.83 (s, H9), 4.27-4.26 (m, H12) ppm **^{13}C NMR (100MHz, DMSO-d6) *δ*:** 156.0 and 153.7(C17, 1JC-F=229.7Hz), 148.8(C14), 146.4(C8), 145.5(C6), 143.2(C1), 134.7(C11), 123.9(C10), 122.0(C3), 119.3(C2), 115.77 and 115.55(C16,18, 2JC-F=21.8Hz), 113.59 and 113.51(C15,19, 3JC-F=8Hz), 119.3(C5), 60.2(C9), 47.6(C12) ppm (*Figure 3.52, 3.53, 3.54*)

H. Molecule **A8**

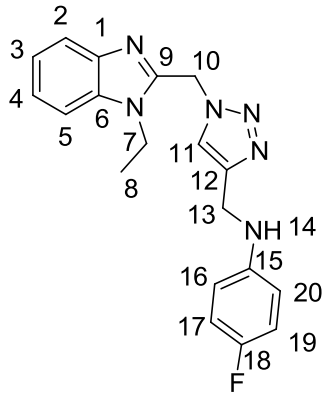	White solid. **Yield:**95% **^{1}H NMR (400MHz,DMSO-d6) *δ*:**8.04 (s, H11), 7.62-7.57 (m, H2, H5), 7.29-7.18(m, H3, H4), 6.91-6.87 (t, H17, H19, *J*=9.2Hz), 6.63-6.59(m, H16, H20), 6.03-6.00 (t, H14, *J*=6Hz), 5.98(s, H10), 4.34-4.30 (q, H7, *J*=7.2Hz), 4.27-4.26 (d, H13, *J*=6Hz), 1.13-1.10(t, H8, *J*=7.2Hz) ppm **^{13}C NMR (100MHz, DMSO-d6) *δ*:**156.0 and 153.7(1JC-F=229.6Hz), 148.4(C15), 146.4(C9), 145.4(C6), 142.4(C1), 135.1(C12), 123.9(C11), 123.1(C4), 122.3(C3), 119.7(C2), 115.73 and 115.52 (2JC-F=21.8Hz), 113.6 and 113.5(C16,C20, 3JC-F=7.3Hz), 110.9(C5), 46.1(C10), 38.7(C7), 15.1(C8) ppm (*Figure 3.57*)

Overall comparing the NMR and getting insight from single crystal we observed that protons falling in the shielded zone are expected to be appear in the shielded zone of NMR spectra as depicted below. This is specially seen for triazole proton, which appears at 8.7ppm for phenyl derivative and at 8.0ppm for aniline derivatives.

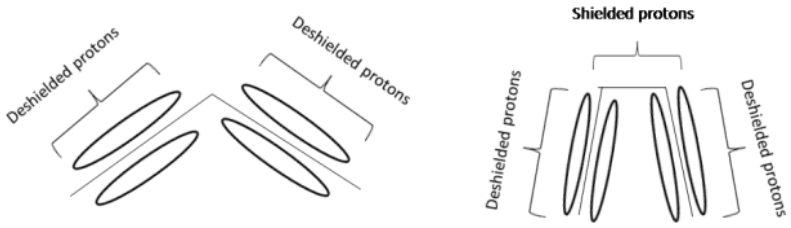

3.6 Objective 5: Systematic NMR studies (Concentration as well as water addition experiment)

Nuclear magnetic resonance (NMR) spectroscopy is one of the most useful techniques available to chemists for the investigation of dynamic molecular processes. Most basic treatments of NMR include atleast a qualitative description of the effect of "exchange" that is reversible dynamic processes, on the appearance of NMR spectra.

As per observation made earlier for the self aggregation, in this section we planned NMR studies in two ways (i) Concentration dependent NMR study and (ii) water addition NMR titrations.

1. Concentration dependent NMR:

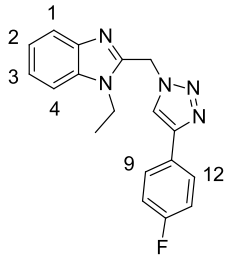

The experiment was performed for molecule **A4**. Molecule **A4** (10mg) was dissolved in DMSO-d6 (0.5ml) and NMR was recorded. NMR was also recorded for 20mg and 30mg of molecule **A4** in same 0.5ml of DMSO-d6. We observed that proton 3 shifts downfield and proton 2 shifts up-field. Also the 1,4 proton splits into two separate doublet starting with a triplet looking peak (Not a true triplet as *J* values are not same for the two fragments in case of 10mg and 20mg experiment).

2. Water addition NMR experiments:

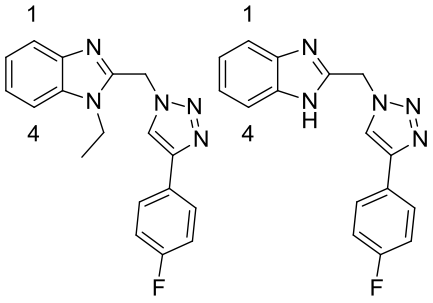

All the molecules **A1** to **A8** (10mg) were dissolved in DMSO-d6 (0.5ml) and the ^{1}H NMR was recorded. Amount of D_2O added during titration is 10, 20, 30, 30, 30, 30 and 30µl to the NMR tube and then ^{1}H NMR was recorded. *Figure 3.30* shows the comparative water addition NMR of ethyl derivative **A6** and non ethyl derivative **A7**. This clearly shows that 1,4 protons in case of ethyl derivative showed merged to separated peaks, on the other hand non-ethyl derivative **A7** showed separated to merged signals for the same protons. For all other molecules NMR is presented in selected spectra section.

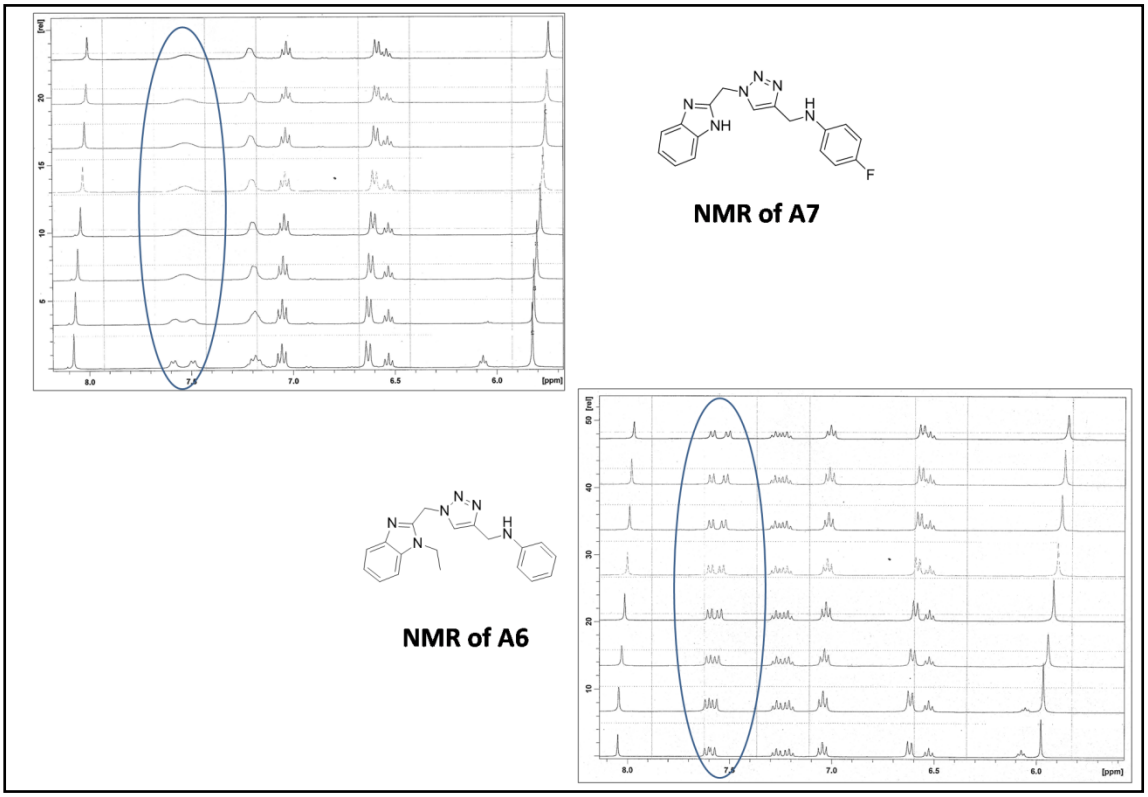

Figure 3.30: ^{1}H NMR of water addition experiment on A6 and A7

Observations from Water addition NMR experiment (*Table 3.3*):

- Methyl peak: Aniline derivatives have more up-field shifting as compared to phenyl derivative.
- Water: Downfield shift is more in aniline derivative as compared to phenyl derivative.

- CH_2 imidazole linker: Shifting is more prominent with ethyl derivatives as compared with non-ethyl ones.
- Triazole ring proton: Shifting is more for phenyl rings as compared to aniline rings.
- Ortho phenyl ring protons: Shifting is more for phenyl ring derivatives.
- 1,4-benzimidazole ring protons:
  (a) Phenyl and phenyl ethyl protons shows single peak for the two, rest cases shows two different peaks.
  (b) 1 remains constant and 4 shifts for ethyl derivatives and 4 remains constant and 1 shift for non-ethyl derivatives.
  (c) For ethyl derivatives initially peaks are merged and then splitting occurs, for non-ethyl derivatives initially peak is separated and then it merges.

Table 3.3: Observations for shifting of peaks from water addition NMR experiment:

S.No	Peaks under consideration	Aniline (A5,A6,A7,A8)	Non-aniline (A1,A2,A3,A4)	Ethyl (A2,A4,A6,A8)	Non-Ethyl (A1,A3,A5,A7)
1	Methyl	More (Double, Upfield)	Less		
2	Water	More (0.100 ppm, downfield shift)	Less		
3	CH_2 imidazole linker			More (30%)	Less
4	Triazole Ring	Less	More (Almost Double)		
5	O-phenyl ring	Less	More (Almost double)		

6	1,4-benzimidazole			1(Constant),4(Shifts Up-field) [Merged to Separate]	4(Constant), 1(Shifts Up-field)[Separated to merged]

All the eight molecules are inherently flexible due to the nature of the single bonds connecting the benzimidazole arm to the central triazole ring. As a result, they are likely able to adopt a number of conformations separated by low energetic barriers.This is especially true in organic solutions like dimethyl sulfoxide (DMSO) where the greasy aromatic elements of the hosts are well solvated. In D_2O however, the geometries adapted will depend on the inherent bond rotational preferences of the molecules (as in DMSO) as well as aromatic clustering driven by the hydrophobic effect.

These observations are the result of molecular dynamics in solution phase. As observed from NMR that 1,4 protons behave differently for ethyl and non-ethyl derivatives (*Figure3.29*). (i) It is clearly observed that by adding D_2O to the NMR tube, the 1,4 protons for ethyl derivatives initially showed single peak and then they separate. This can be explained when by the locking of rotation of the molecules. (ii) On the other hand for non-ethyl molecules the peaks are initially separated and they merge on addition of water. This can be explained by fast tumbling of molecules as we add smaller polar solvent to thesystem.

3.6 Conclusion:

Benzimidazole linked triazole molecule, heterocyclic compound, has many non- covalent interacting sites which are responsible for self aggregation. To tune this self aggregation behavior we designed eight different molecules. Our present understanding shows self aggregation behavior for all eight molecules. Insertion of ethyl group on nitrogen of benzimidazole molecule changed aggregation growth behavior from spherulitic to fibrillar. Molecular signature for this behavior was probed using concentration and water dependent NMR studies. Although here NMR studies shows contradictory behavior for all the four non-ethyl and all four ethyl derivatives, more studies are required to probe the molecular level understanding. On this line few important observations we can quote from our experiments.

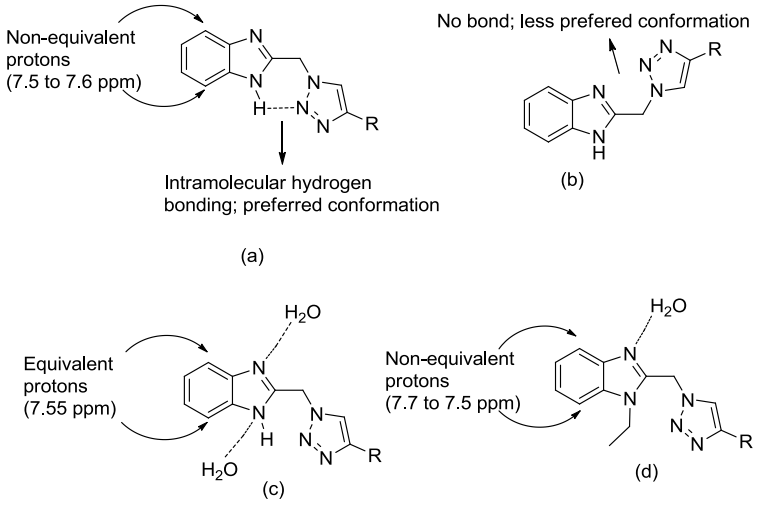

Figure3.31: (a) Intramolecular hydrogen bond making 1,4-protons non-equivalent, (b) structure on free rotation along CH_2 linker, (c) after water addition equivalency of two N's of benzimidazole ring and (d) after water addition non-equivalency of ethyl derivative

- All eight molecules showed fiber formation, during experimental conditions, where stable at room temperature for 6 to 7 days and their formation is thermoreversible.
- Polarizing optical microscopy helped in observing the morphology of this fiber formation or self aggregation. Both, sphirulitical and fibrillar growth were observed followed by tip branching and side branching. Out of the representative

four molecules, we observed fibrillar growth for non-ethyl derivative and spherulitical growth for rest of the three ethyl derivatives.

- Thermal studies, TG-DTA and DSC, showed phase transition in three representative molecules in the temperature range at between 125°C-200°C.
- Single crystal XRD study disclosed '*pro*-aggregation' topology for few Hydrogen atoms in the molecule in the solid state, which latter confirmed in the solution NMR study.
- Detailed complete assignment of the protons for all the eight molecules was carried out using COSY and HSQC NMR experiments.
- Two distinct NMR experiments carried out by (i) changing concentration, and (ii) addition of water in DMSO. Both the experiments reveal the systematic shifting of protons positions, such as methylene bridges, *ortho*protons of the phenyl ring.
- Both these NMR experiments showed splitting of 1,4 peak in **A4**, 1-ethyl-2-((4-(4-fluorophenyl)-1H-1,2,3-triazol-1-yl)methyl)-1H-benzo[d]imidazole (floro ethyl derivative), confirming their role in aggregation.
- As observed from NMR that 1,4 protons behave differently for ethyl and non-ethyl derivatives. (i) It is clearly observed that by adding D_2O to the NMR tube, the 1,4 protons for ethyl derivatives initially showed single peak and then they separate. This can be explained when by the locking of rotation of the molecules. (ii) On the other hand for non-ethyl molecules the peaks are initially separated and they merge on addition of water. This can be explained by fast tumbling of molecules as we add smaller polar solvent to the system (Figure 3.31).
- The slight down-field shifting of 2^{nd} proton and up-field shifting of 3^{rd} proton, benzimidazole ring hyodrogens 5 and 6 respectively, plays critical role in aggregation behavior, which is also observed in single crystal data.

3.7 Experimental

3.7.1 Materials and Methods:

All the compounds were purified using column chromatography (2000- 400 mesh silica) before characterization. TLC analysis was done using pre-coated silica on aluminum sheets. Melting points were recorded in Thiele's tube using paraffin oil and are uncorrected. FT-IR (KBr pellets) spectra were recorded in the 4000-400 cm^{-1} range using a Perkin-Elmer FT-IR spectrometer. The NMR spectra were obtained on a Bruker AV-III 400 MHz spectrometer using TMS as an internal standard. The chemical shifts were reported in parts per million (ppm), coupling constants (J) were expressed in hertz (Hz) and signals were described as singlet (s), doublet(d), triplet(t), broad (b) as well as multiplet (m). The microanalysis was carried out using a Perkin-Elmer IA 2400 series elemental analyzer. The mass spectra were recorded on Thermo scientific DSQ-II. All chemicals and solvents were of commercial grade and were used without further purification. Single crystal data was collected with Xcalibur, EoS, Gemini.

3.7.2 Synthesis of compounds:

Synthetic procedures are reported in chapter 2.2. Briefly click reactions were used to form 1,2,3-triazole ring. Two pharmacophores in all were incorporated in the system; benzimidazole and triazole ring.

3.8 Selected Spectra

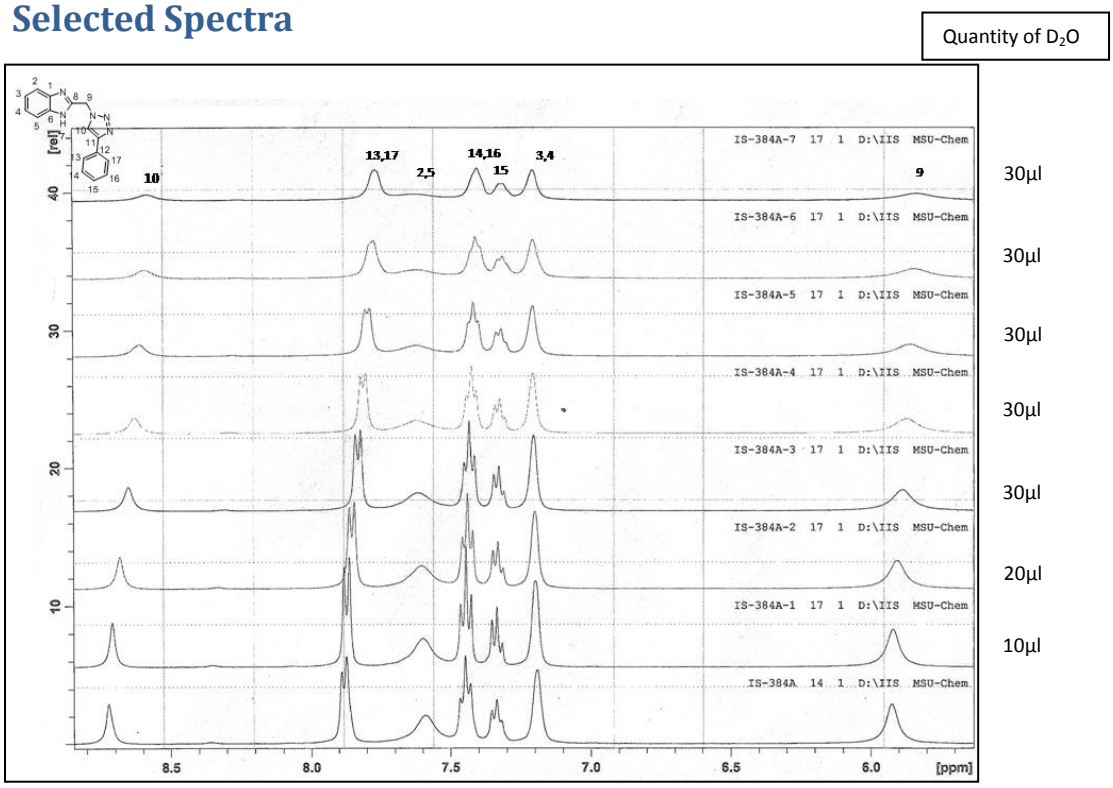

Figure 3.32: ^{1}H NMR spectra of A1

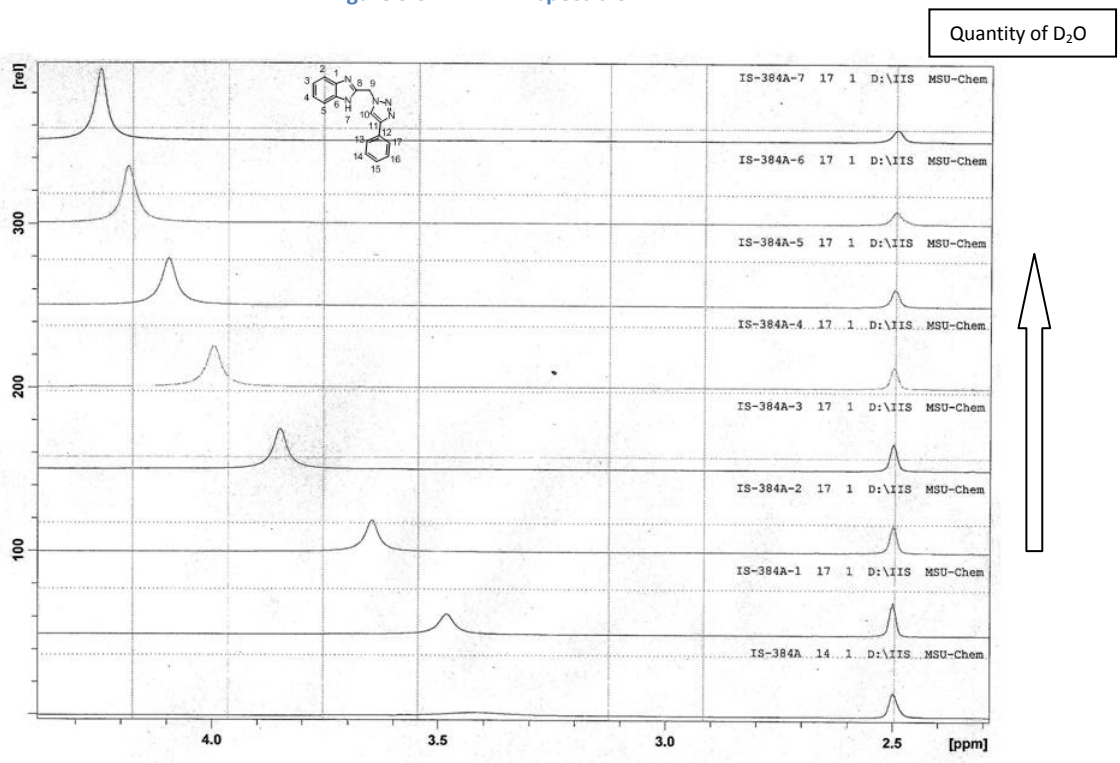

Figure 3.33: ^{1}H NMR spectra of A1

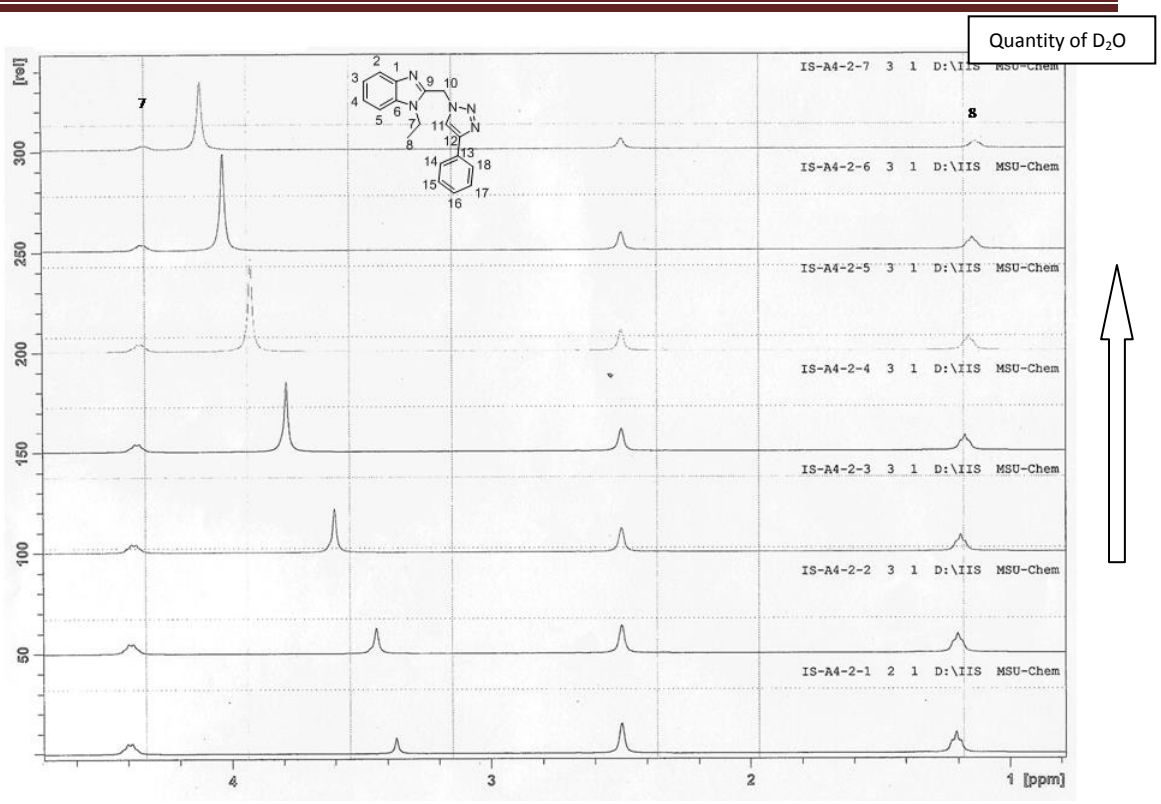

Figure 3.34: ^{1}H NMR spectra of A2

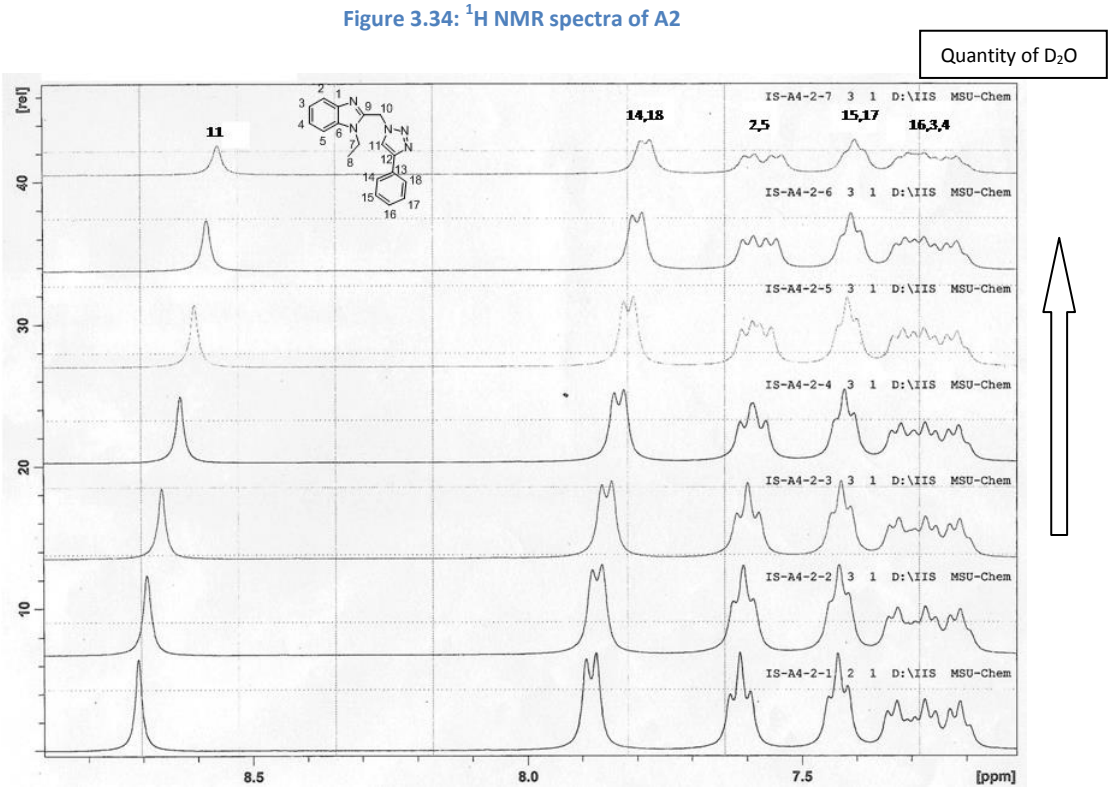

Figure 3.35: ^{1}H NMR spectra of A2

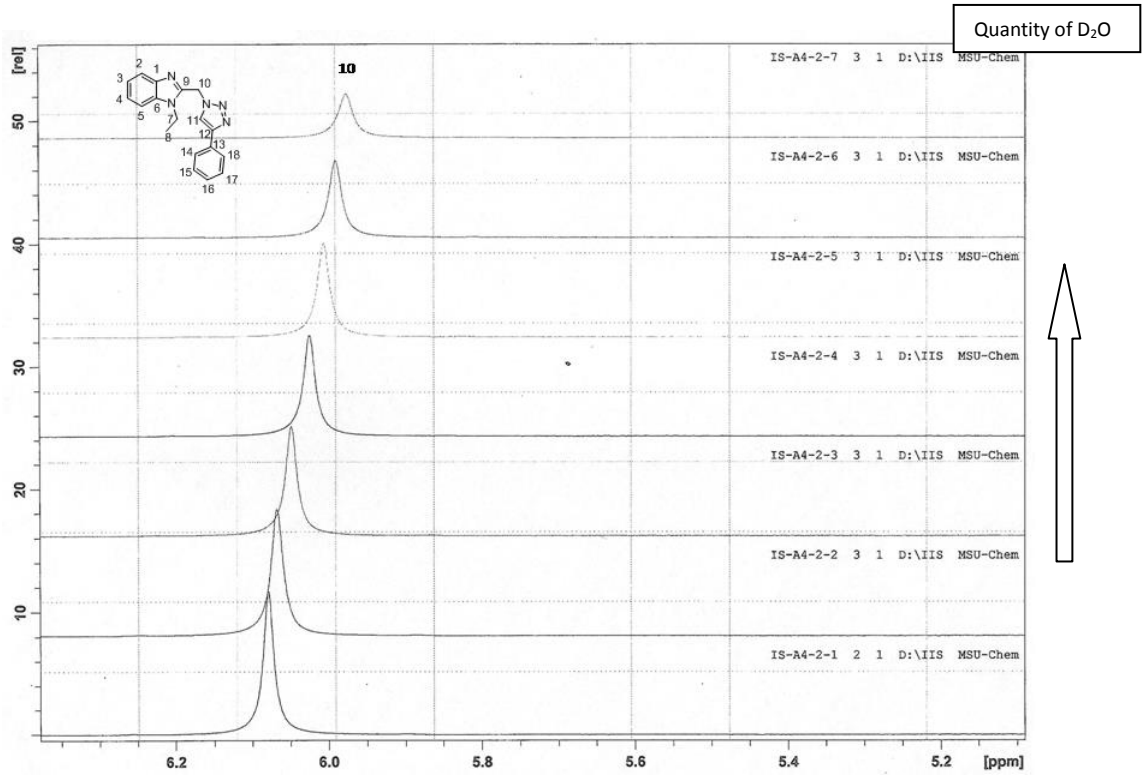

Figure 3.36: ^{1}H NMR Spectra of A2

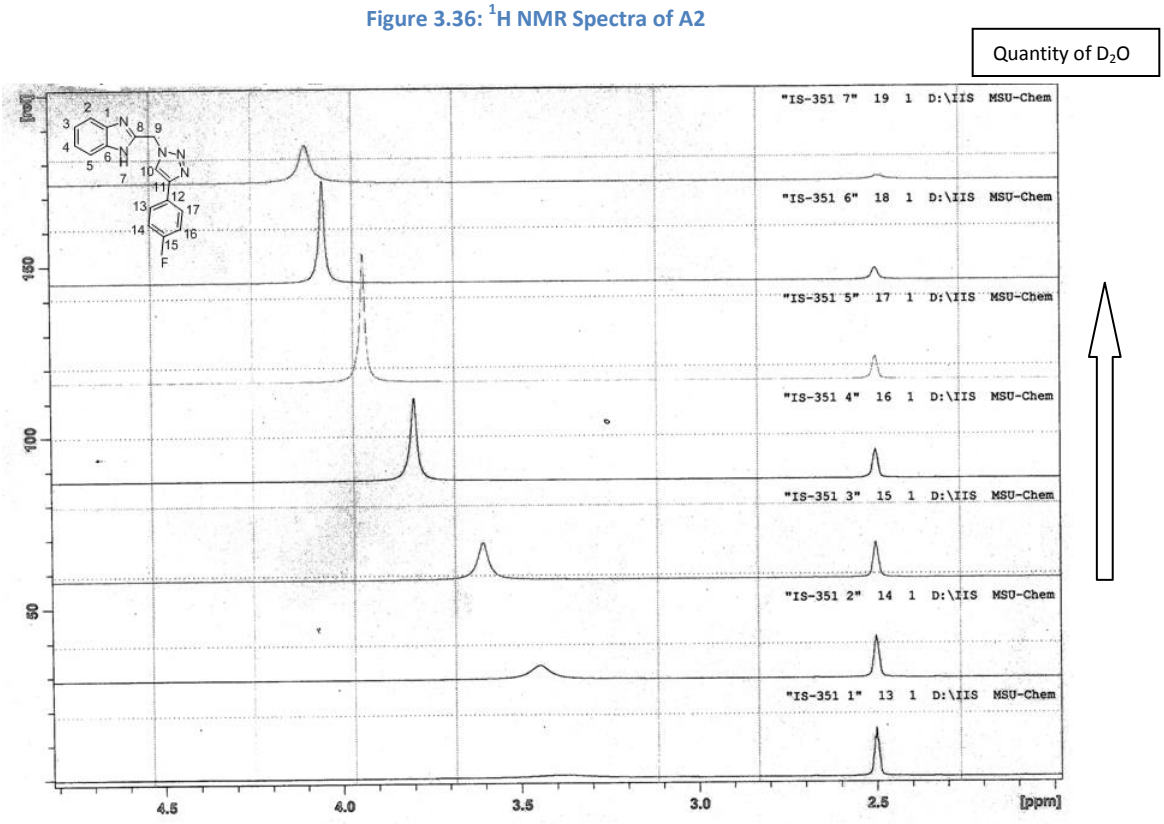

Figure 3.37: ^{1}H NMR spectra of A3

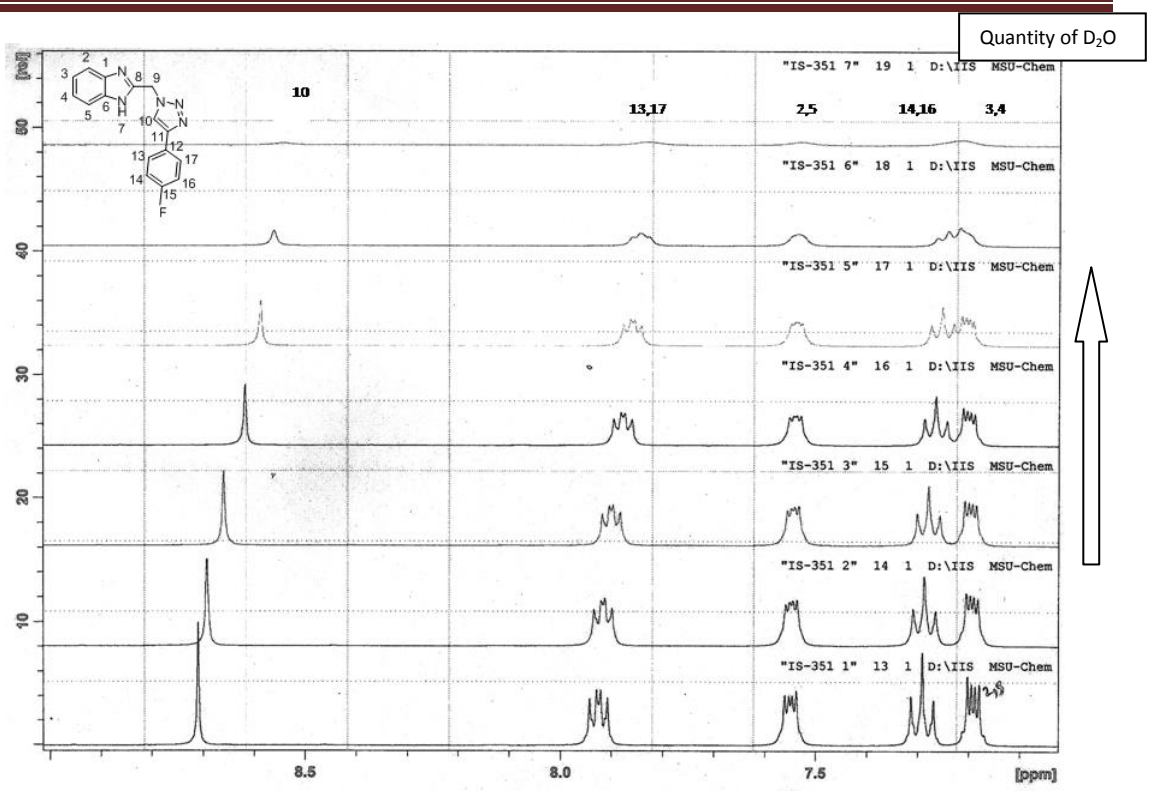

Figure 3.38: ^{1}H NMR spectra of A3

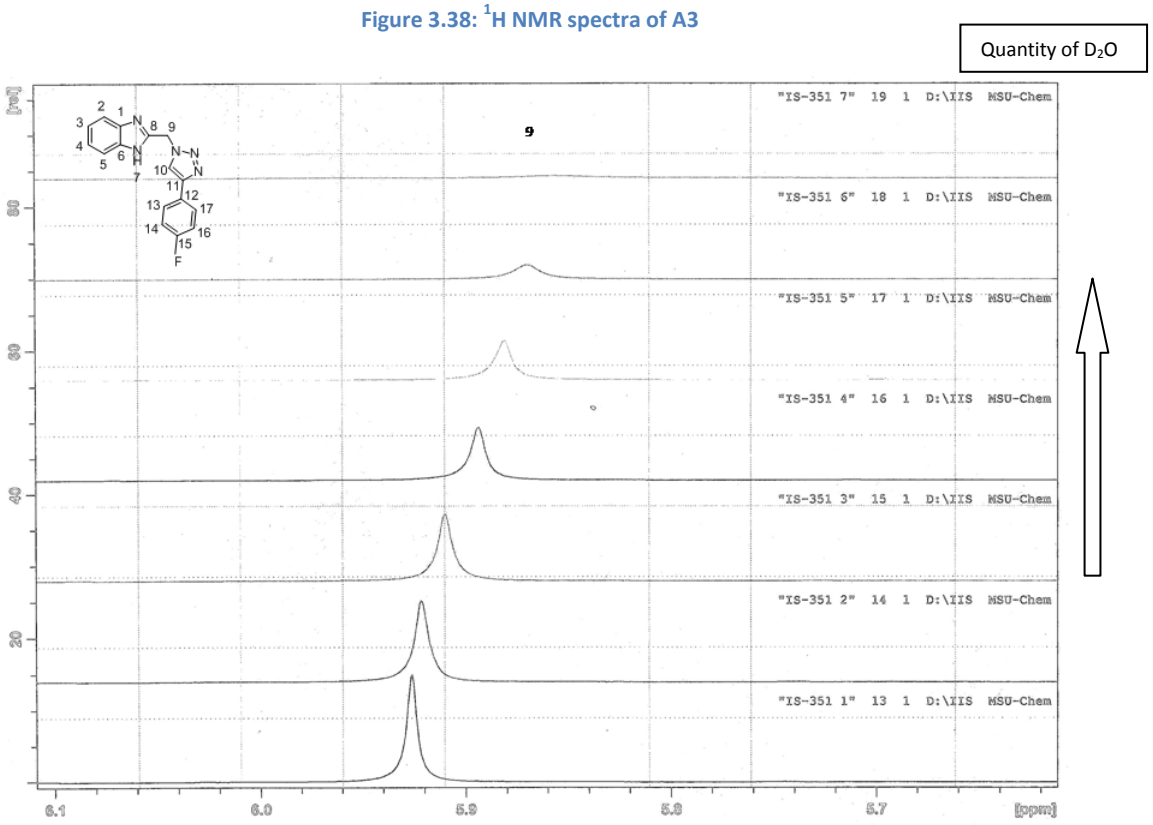

Figure 3.39: ^{1}H NMR spectra of A3

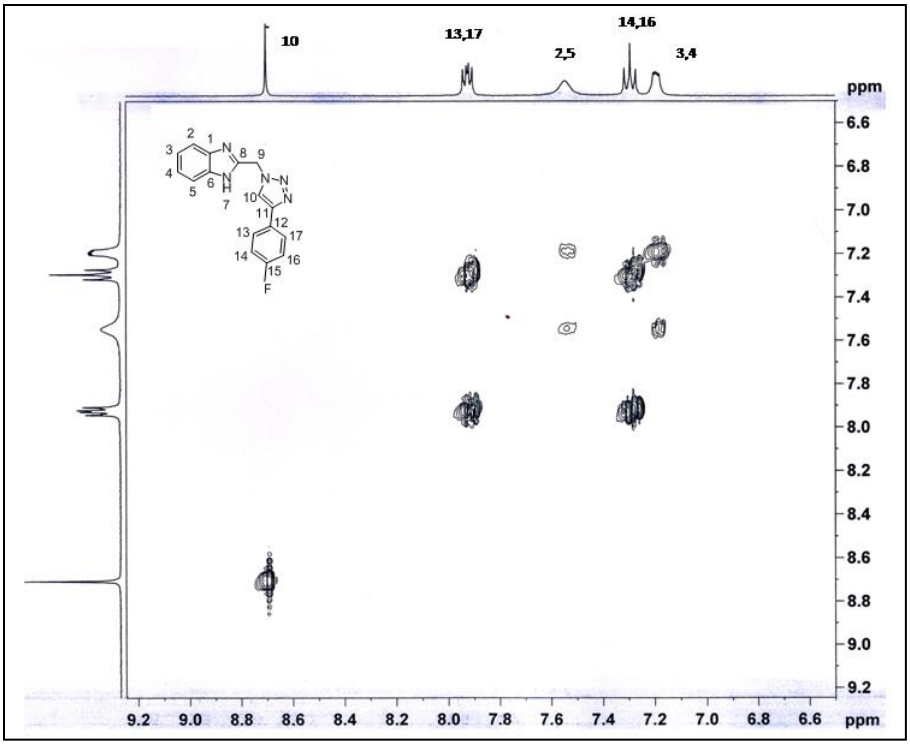

Figure 3.40: COSY of A3

Quantity of D_2O

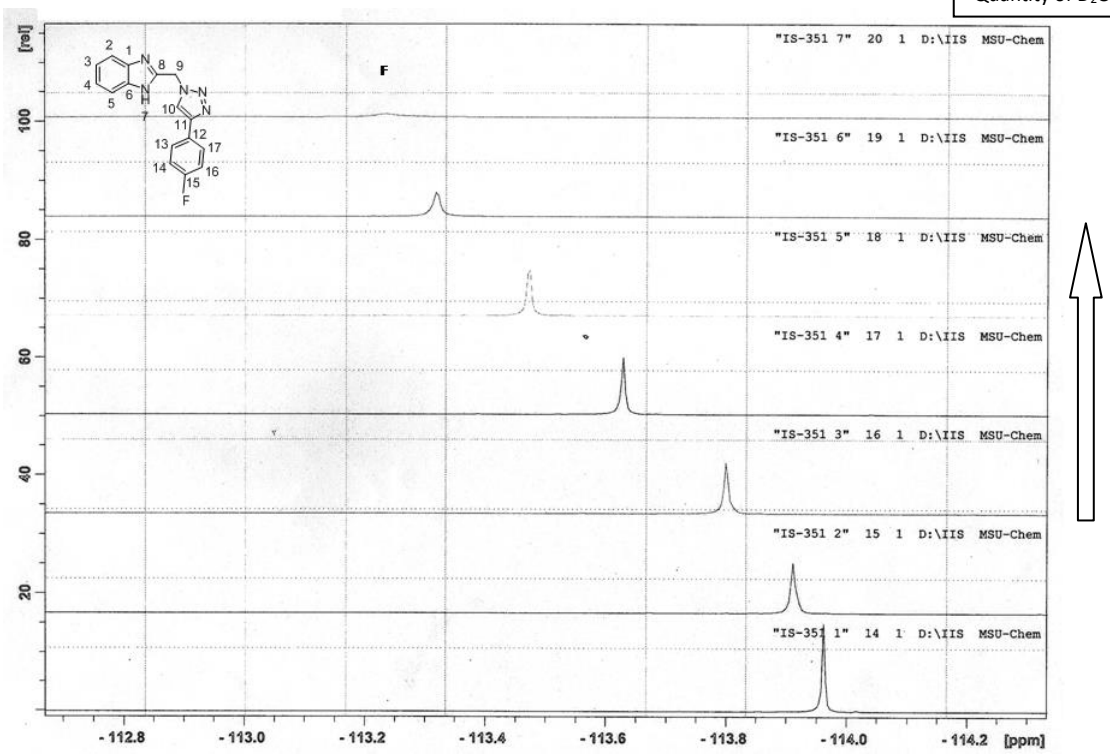

Figure 3.41: ^{19}F NMR spectra of A3

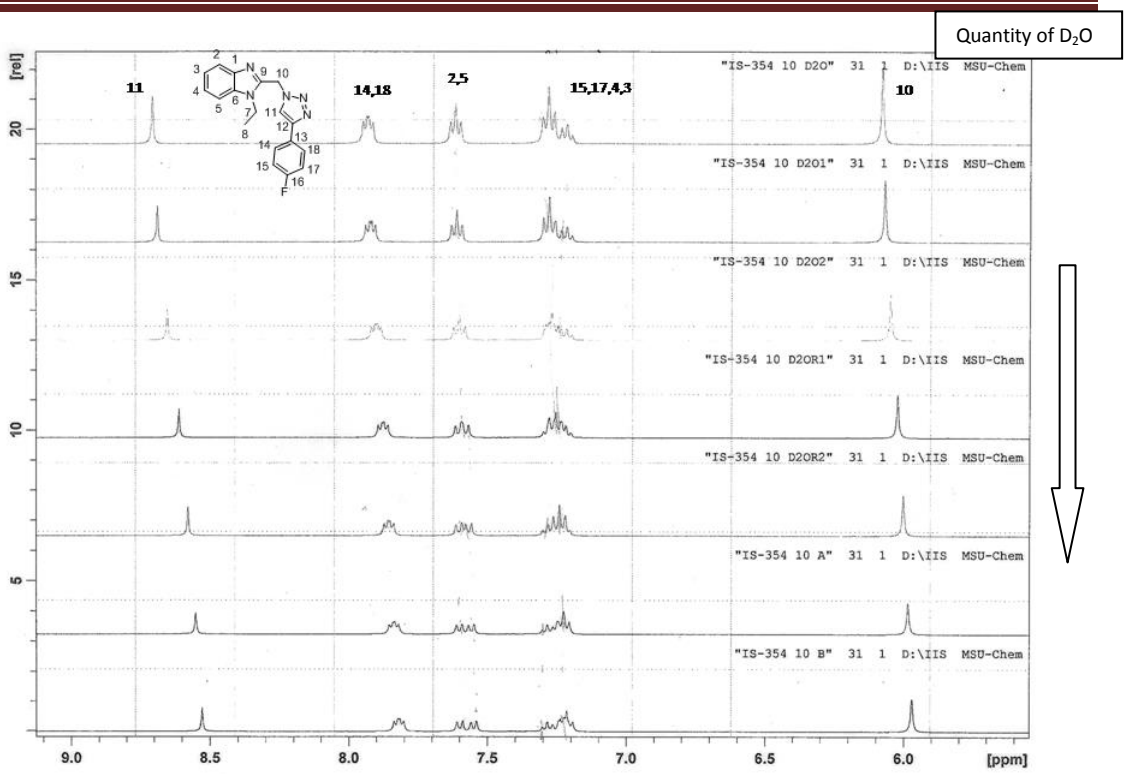

Figure 3.42: ^{1}H NMR spectra of A4

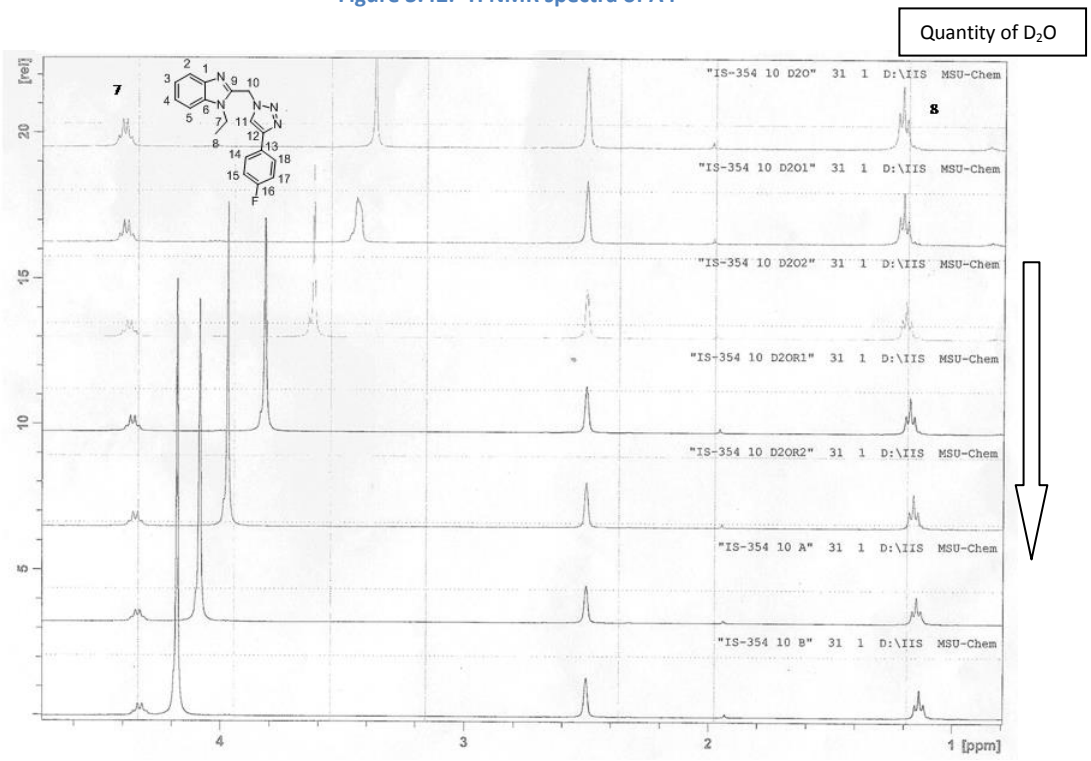

Figure 3.43: ^{1}H NMR spectra of A4

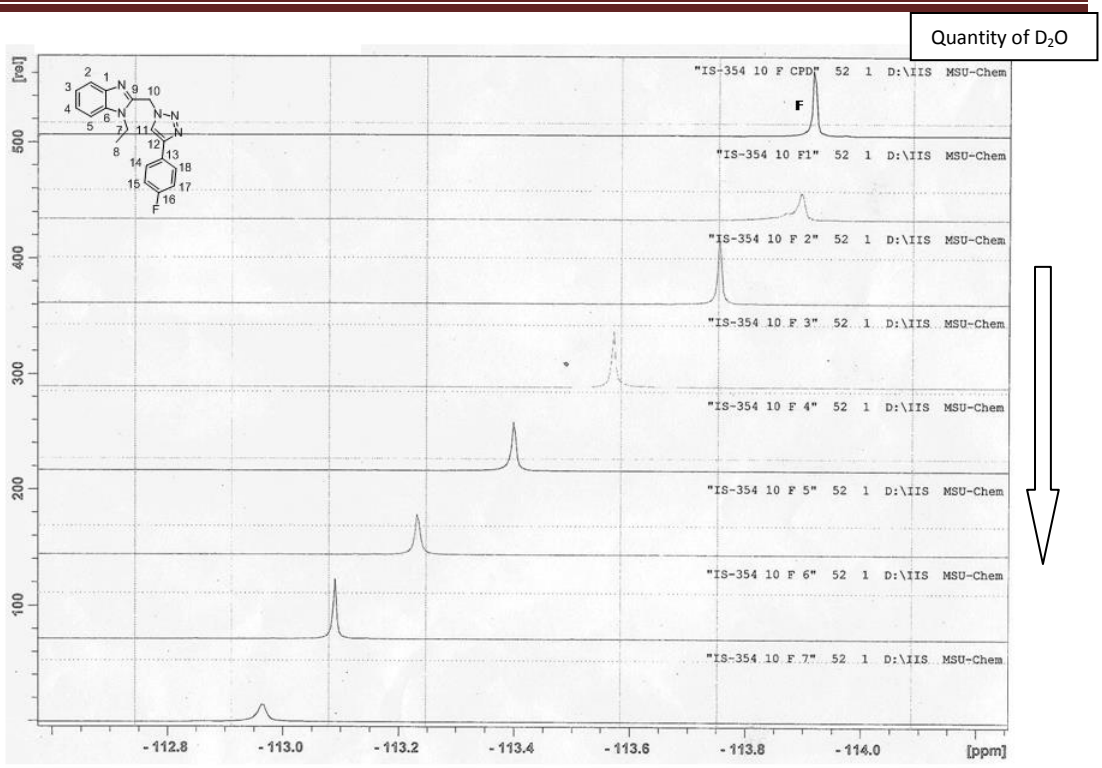

Figure 3.44: ^{19}F NMR spectra of A4

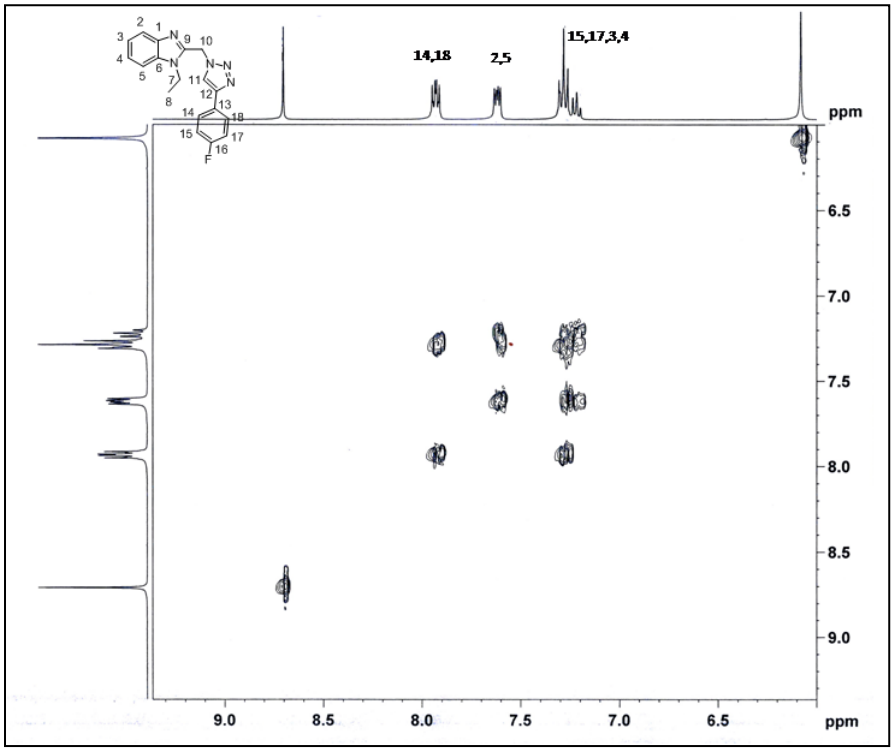

Figure 3.45: COSY spectra of A4

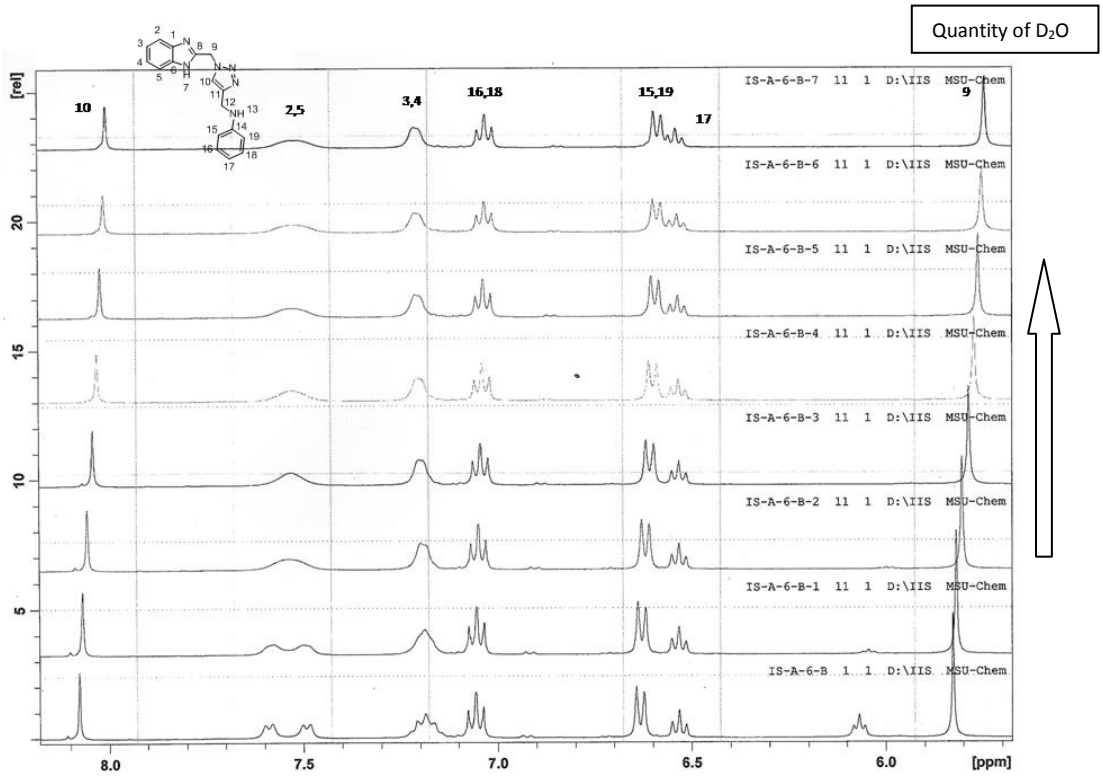

Figure 3.46: ^{1}H NMR spectra of A5

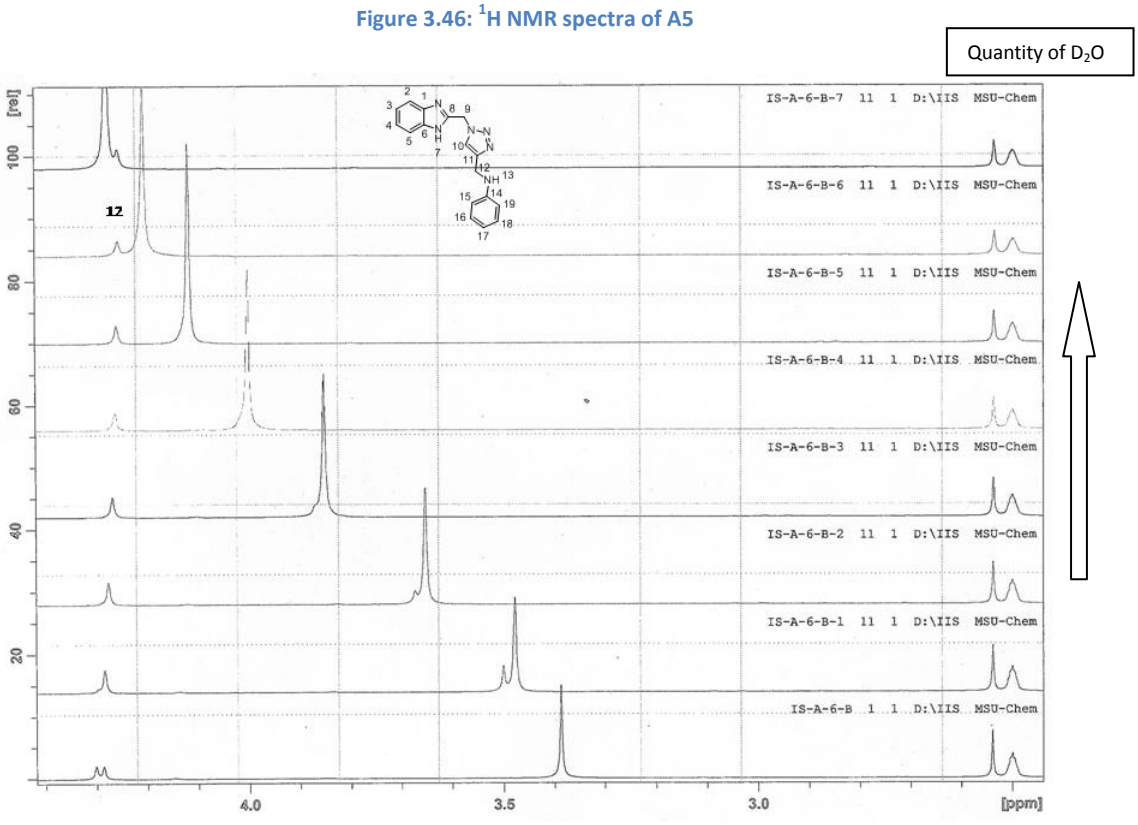

Figure 3.47: ^{1}H NMR spectra of A5

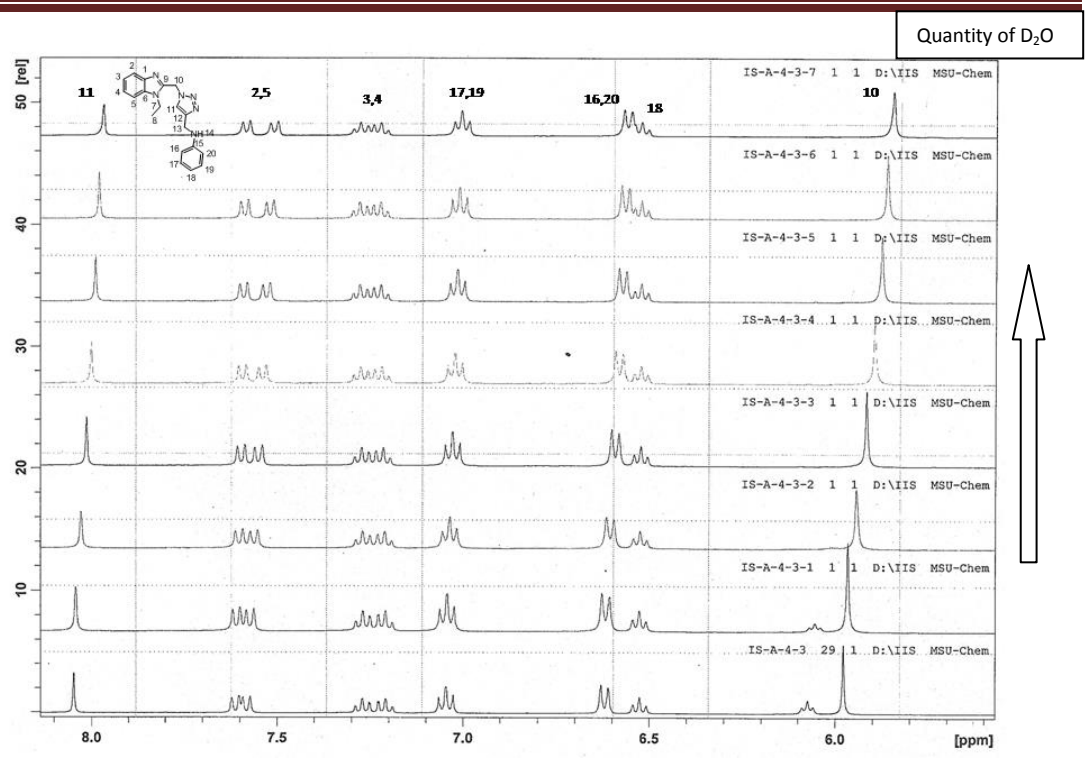

Figure 3.48: ^{1}H NMR spectra of A6

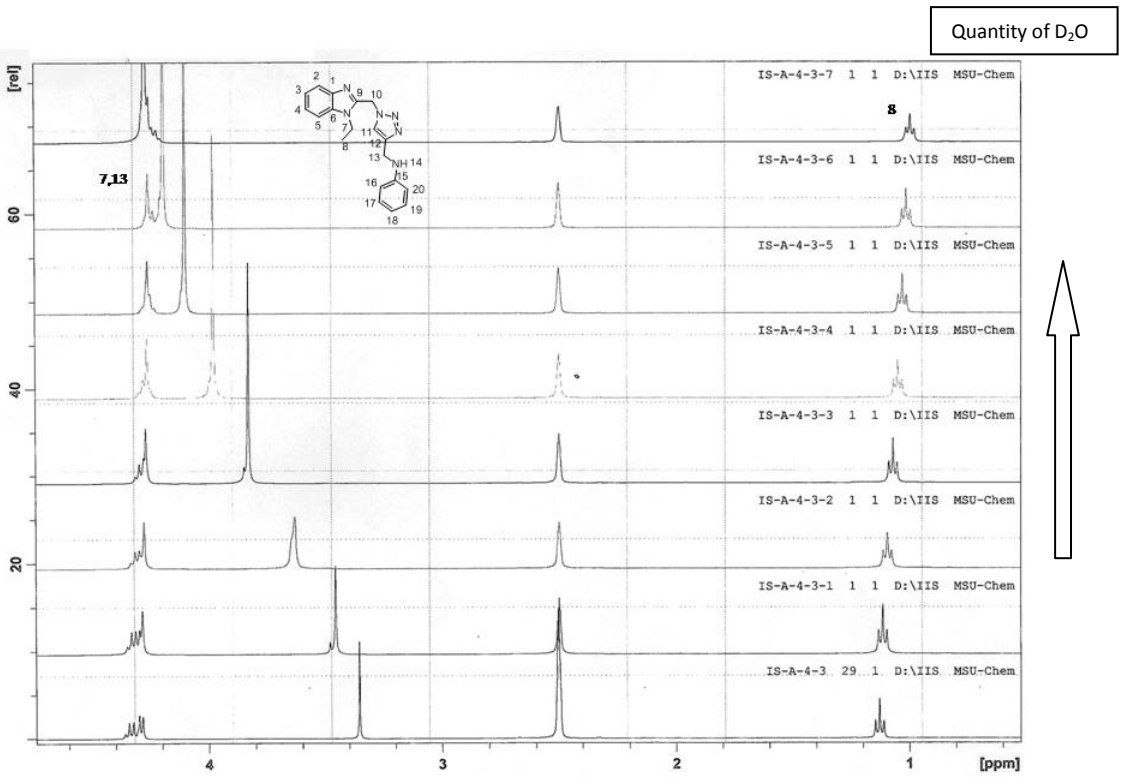

Figure 3.49: ^{1}H NMR spectra of A6

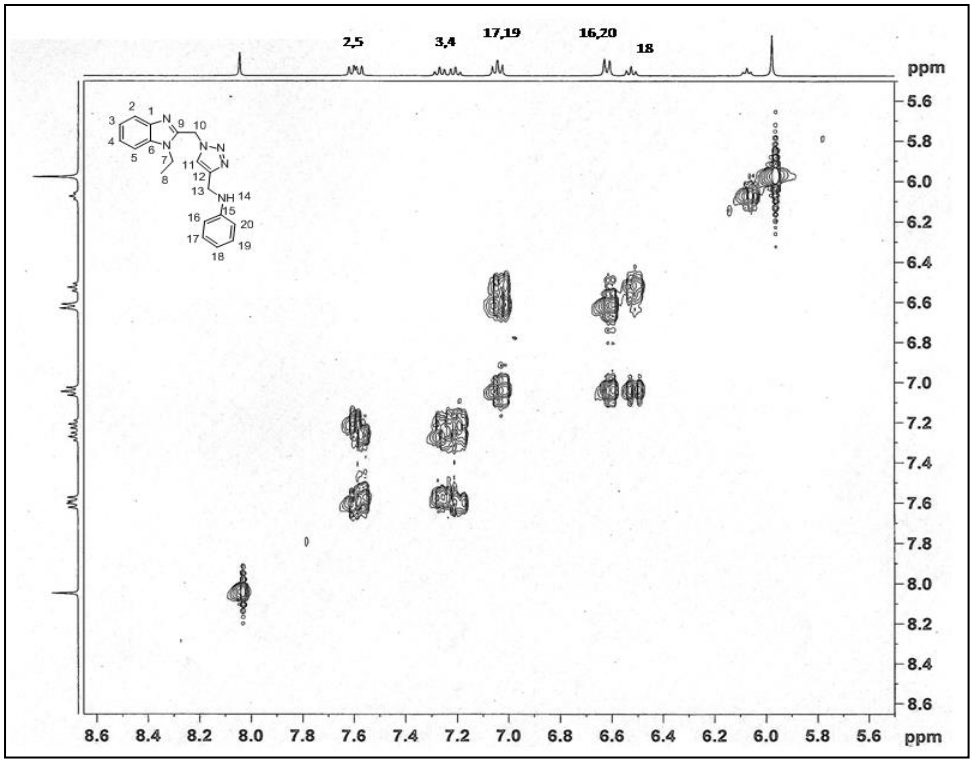

Figure 3.50: COSY spectra of A6

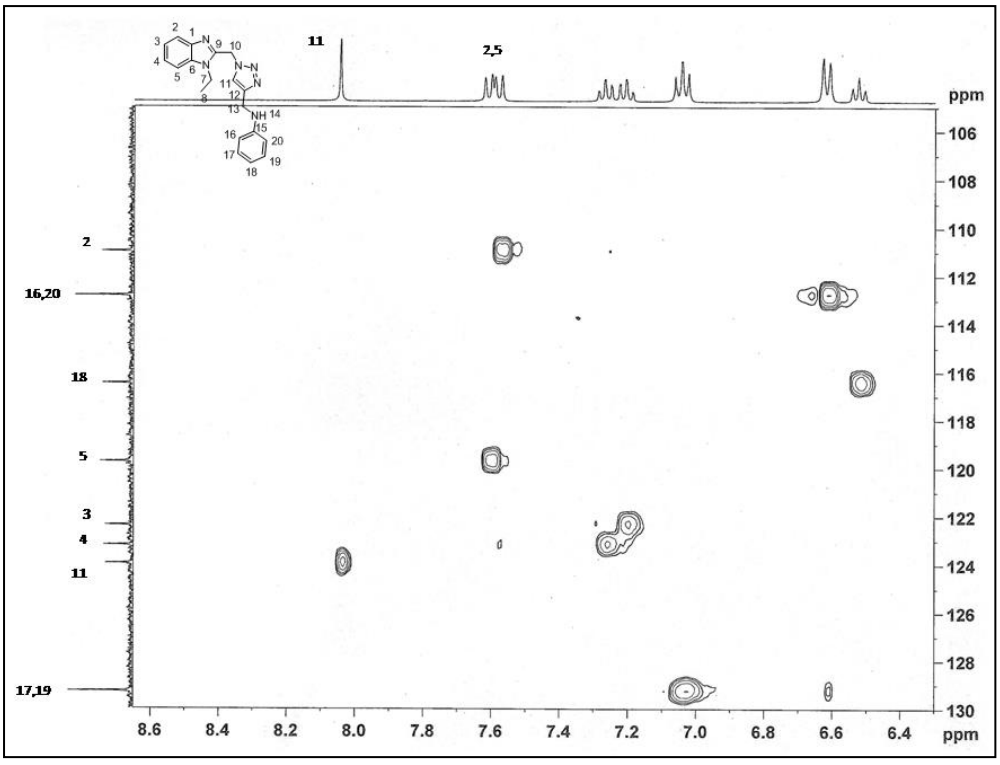

Figure 3.51: HSQC of A6

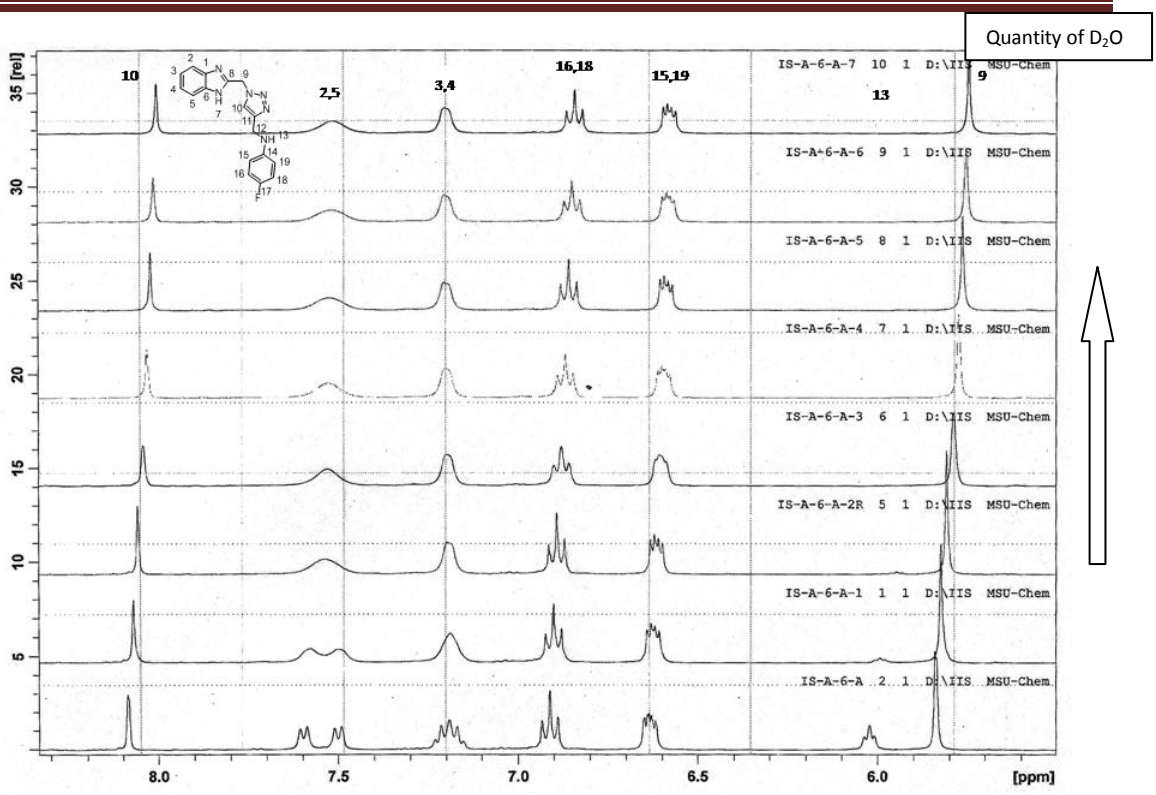

Figure 3.52: ^{1}H NMR of A7

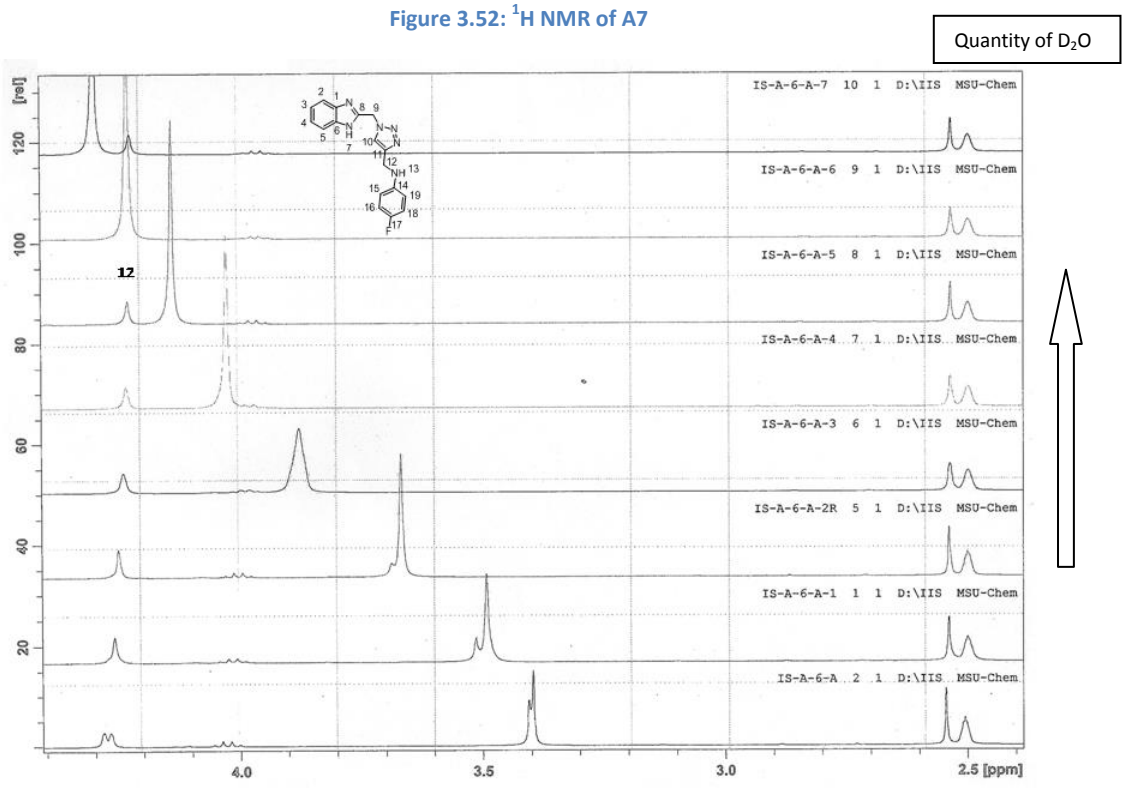

Figure 3.53: ^{1}H NMR of A7

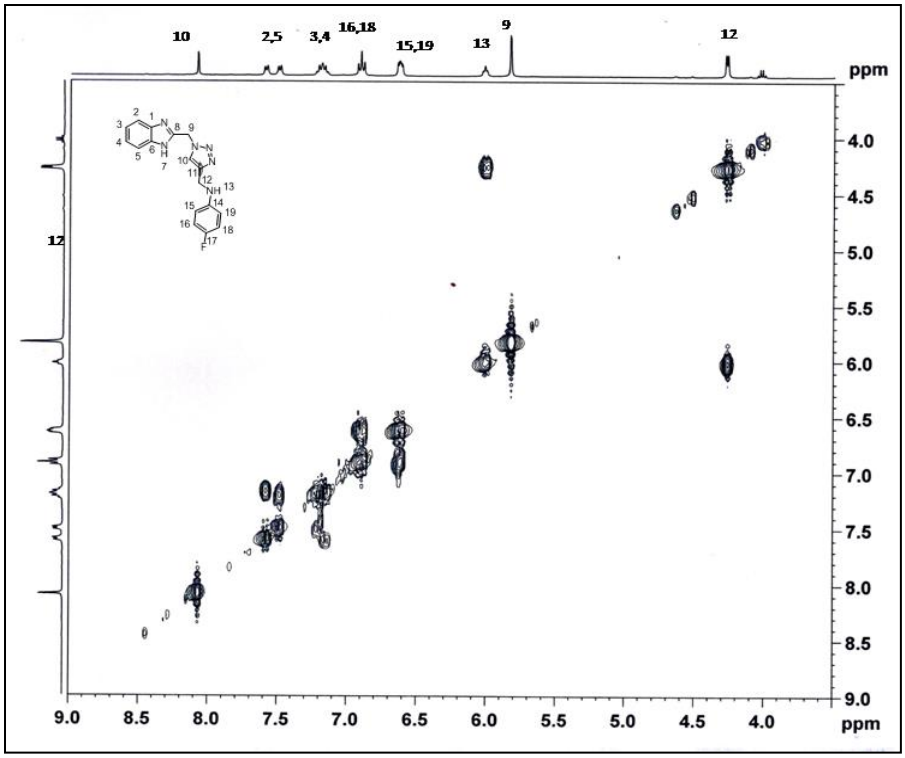

Figure 3.54: COSY of A7

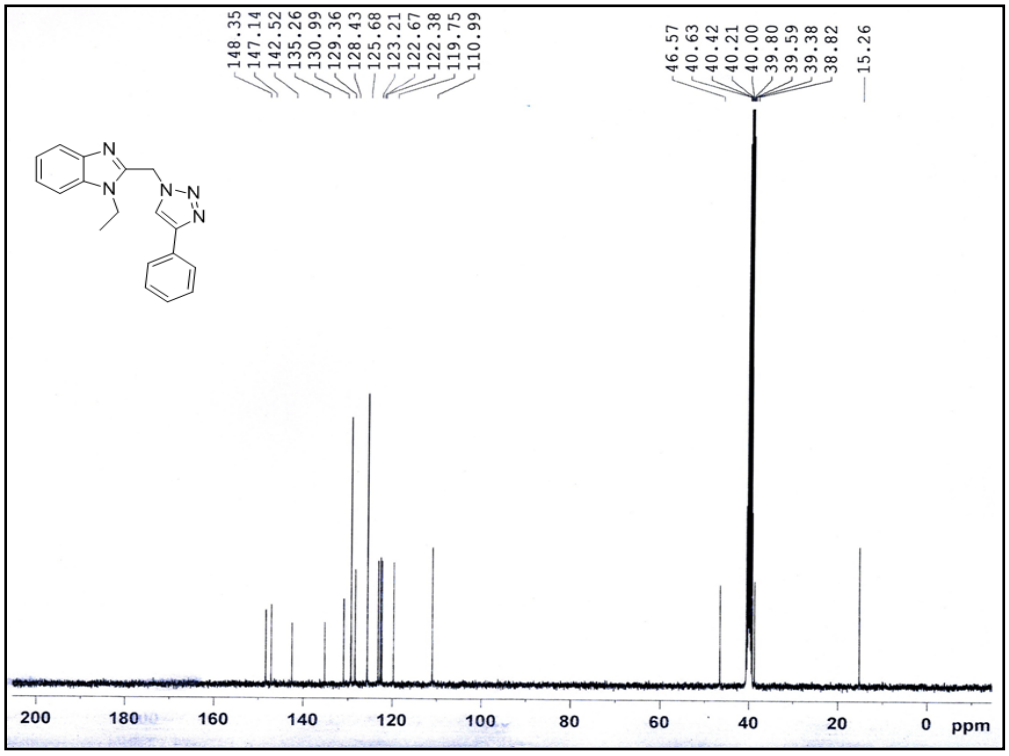

Figure 3.55: ^{13}C NMR spectra of A2

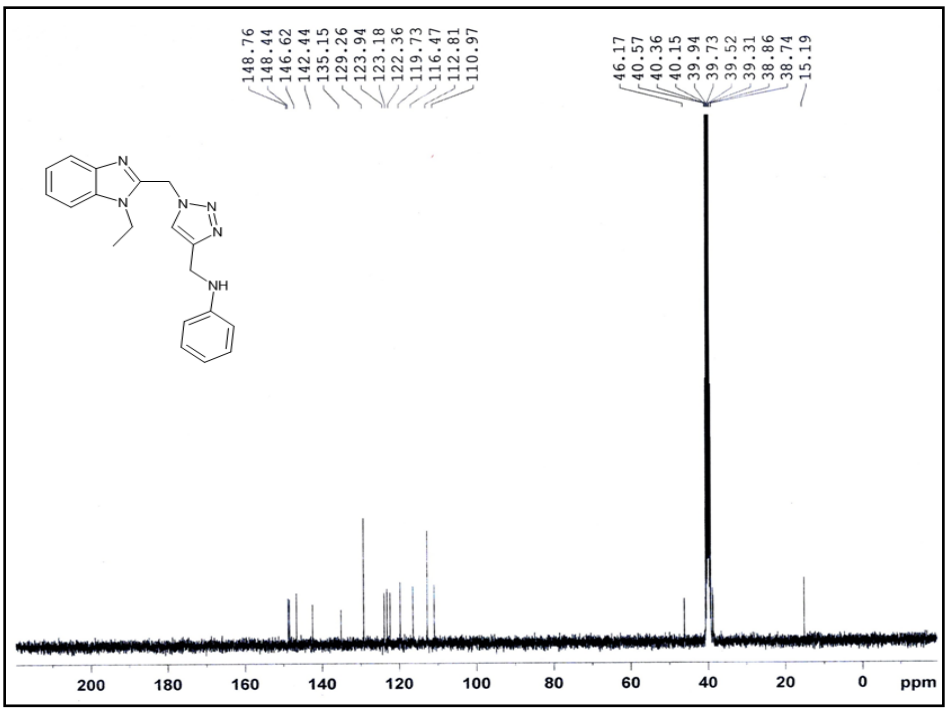

Figure 3.56: ^{13}C NMR of A6

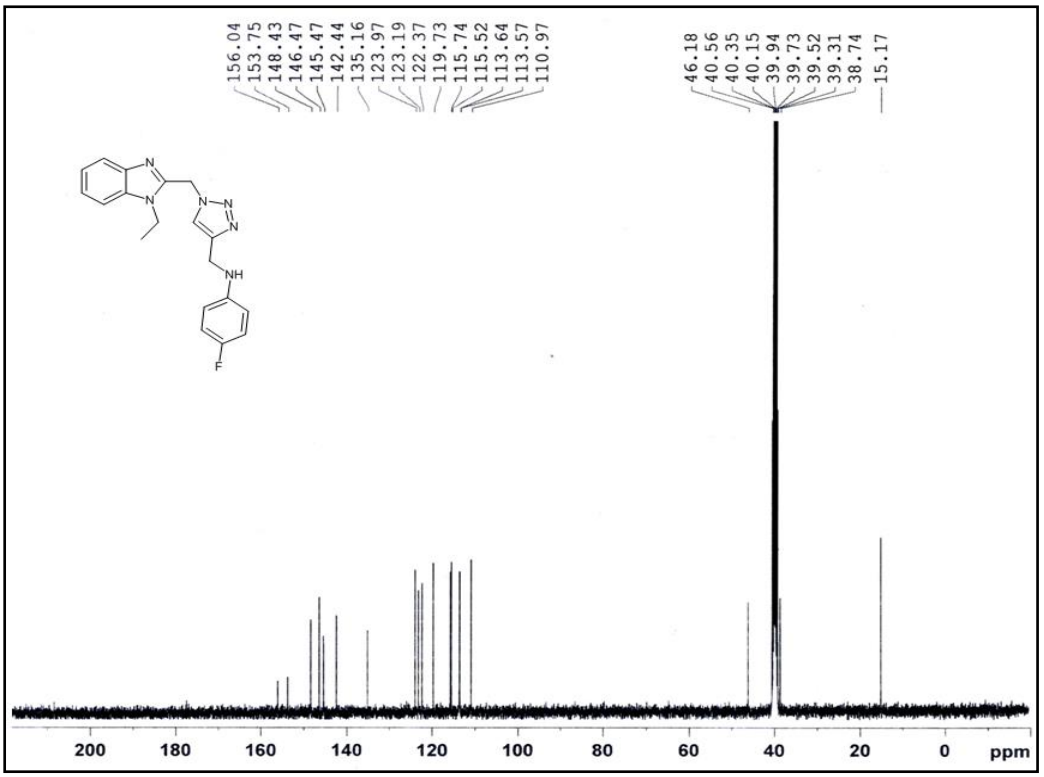

Figure 3.57: ^{13}C NMR of A8

3.9 Reference:

[1] Okesola, B.O.; Smith, D.K. *Chemical Society Reviews*, **2016**, *45*, 4226-4251.

[2] Cheng, N.; Hu, Q.; Guo, Y.; Wang, Y.; Yu, L. *ACS applied materials & interfaces*, **2015**, *7*, 10258-10265.

[3] Wang, J.; Wang, H.; Song, Z.; Kong, D.; Chen, X.; Yang, Z. *Colloids and Surfaces B: Biointerfaces*, **2010**, *80*, 155-160.

[4] Wang, G.; Cheuk, S.; Yang, H.; Goyal, N.; Reddy, P. N.;Hopkinson, B. *Langmuir*, **2009**, *25*, 8696-8705.

[5] Mangunuru, H.P.; Yerabolu, J. R.; Liu, D.;Wang, G. *Tetrahedron Letters*, **2015**, *56*, 82-85.

[6] Caran, K. L.; Lee, Dong-C.; Weiss, R. G.; Molecular Gels and Their Fibrillar Networks, In *Soft Fibrillar Materials: Fabrication and Applications*, First Edition, Liu, X. Y., Li, Jing-L.; Wiley-VCH Verlag GmbH and Co. KGaA, **2013**; 3-75.

[7] Terech, P.; Weiss, R. G. *Chemical reviews*, **1997**, *97*, 3133-3160.

[8] Catalan, J.; Diaz, C.; Garcia-Blanco, F. *The Journal of organic chemistry*, **2001**, *66*, 5846-5852.

[9] Wallace, V. M.; Dhumal, N. R.; Zehentbauer, F. M.; Kim, H. J.; Kiefer, J. *The Journal of Physical Chemistry B*, **2015**, *119*, 14780-14789.

[10] Shen, X.; Jiao, T.; Zhang, Q.; Guo, H.; Lv, Y.; Zhou, J.; Gao, F. *Journal of Nanomaterials*, **2013**, 2.

[11] Sambanthamoorthy, K.; Gokhale, A. A.; Lao, W.; Parashar, V.; Neiditch, M. B.; Semmelhack, M. F.; Lee, I.; Waters, C. M. *Antimicrobial agents and chemotherapy*, **2011**, *55*, 4369-4378.

[12] Geiger, H.C.; Zick, P. L.; Roberts, W. R.; Geiger, D. K. *Acta Crystallographica Section C: Structural Chemistry*, **2017**, *73*, 350-356.

[13] Liu, M.; Kira, A.; Nakahara, H. *Langmuir*, **1997**, *13*, 4807-4809.

[14] Liu, M.; Cai, J. *Langmuir*, **2000**, *16*, 2899-2901.

[15] Guo, P.; Liu, M. *Langmuir*, **2005**, *21*, 3410-3412.

[16] Estroff, L. A.; Hamilton, A. D. *Chemical reviews*, **2004**, *104*, 1201-1218.

[17] Lee, K. Y.; Mooney, D. J. *Chemical reviews*, **2001**, *101*, 1869-1880.

[18] Xing, B.; Yu, C. W.; Chow, K. H.; Ho, P. L.; Fu, D.; Xu, B. *Journal of the American Chemical Society*, **2002**, *124*, 14846-14847.

[19] Wang, R. Y.; Liu, X. Y.; Narayanan, J.; Xiong, J. Y.; Li, J. L. *The Journal of Physical Chemistry B*, **2006**, *110*, 25797-25802.

[20] Wang, R.; Liu, X. Y.; Xiong, J.; Li, J. *The Journal of Physical Chemistry B*, **2006**, *110*, 7275-7280.

[21] (a) Geiger, C.; Stanescu, M.; Chen, L.; Whitten, D. G. *Langmuir*, **1999**, *15*, 2241-2245. (b) Terech, P.; Allegraud, J. J.; Garner, C. M. *Langmuir*, **1998**, *14*, 3991-3998.

[22] (a) Lescanne, M.; Colin, A.; Mondain-Monval, O.; Fages, F.; Pozzo, J. L. *Langmuir*, **2003**, *19*, 2013-2020. (b) Lescanne, M.; Grondin, P.; d'Aléo, A.; Fages, F.; Pozzo, J. L.; Monval, O. M.; Reinheimer, P.; Colin, A.*Langmuir*, **2004**, *20*, 3032-3041.